Reduced In-Plane, Low Frequency Noise of an Active Flap Rotor

Ben W. Sim
UARC/AFDD
Ames Research Center
Moffett Field, California
ben.w.sim@us.army.mil

Ram D. Janakiram
Flight Technology
The Boeing Company
Mesa, Arizona
ram.d.janakiram@boeing.com

Natasha L. Barbely
Aeromechanics Branch
NASA Ames Research Center
Moffett Field, California
Natasha.Barbely@nasa.gov

Eduardo Solis
Monterey Technologies, Inc.
Monterey, CA 93940
Eduardo.Solis@nasa.gov

ABSTRACT

Results from a recent joint DARPA/Boeing/NASA/Army wind tunnel test demonstrated the ability to reduce in-plane, low frequency noise of the full-scale Boeing-SMART rotor using active flaps. Test data reported in this paper illustrated that acoustic energy in the first six blade-passing harmonics could be reduced by up to 6 decibels at a moderate airspeed, level flight condition corresponding to advance ratio of 0.30. Reduced noise levels were attributed to selective active flap schedules that modified in-plane blade airloads on the advancing side of the rotor, in a manner, which generated counter-acting acoustic pulses that partially offset the negative pressure peaks associated with in-plane, steady thickness noise. These favorable reduced-noise operating states are a strong function of the active flap actuation amplitude, frequency and phase. The associated noise reductions resulted in reduced aural detection distance by up to 18%, but incurred significant vibratory load penalties due to increased hub shear forces. Small reductions in rotor lift-to-drag ratios, of no more than 3%, were also measured.

INTRODUCTION

Operating rotorcraft covertly is important in twenty-first century warfare. Rotorcraft offer strategic opportunities for mobile, close-in observation, support, and attack on either manned or unmanned mobile platforms. As such, stealth and acoustic discretions are prime considerations military helicopters must contend with for mission survivability. Tactical effectiveness of these airborne vehicles lies in their ability to remain concealed. In many ways, this is compromised by the use of lift-generating rotors that produce strong acoustic pressure disturbances (source noise). Low frequency rotor harmonic tones, emitted from near in-plane of the rotor, are particularly of concern[1], as they tend to propagate long distances without substantial reduction in strength due to atmospheric absorption. As such, these low frequency harmonic tones are often responsible for triggering early aural detection, which threaten operational survivability of helicopters.

Recent findings[2] at the U.S. Army Aerofightdynamics Directorate (AFDD), at Ames Research Center, have identified use of advanced rotor designs with active "on-blade" controls as a mean to offer some mitigation of in-plane, low frequency noise. While methods such as Higher Harmonic Control[3] (HHC), Individual Blade Control[4] (IBC), active flap[5] and active twist[6] concepts had been systematically studied for many years, these efforts primarily focused on enhancing rotor performance, reducing vibration and suppressing strong blade-vortex interactions. Effectiveness of these methods lies in their ability to introduce cyclic variations, of two-per-rev or greater, to augment blade motions and blade airloads to achieve specific objectives. In a similar fashion, the noise mitigation approach recently proposed by AFDD makes use of these active controls to modify inherent aerodynamic blade loads to generate an "anti-noise" waveform that offsets the low frequency sounds generated by the rotor. A separate study reported by the University of Maryland[7] also demonstrated the possibility and feasibility of achieving low frequency noise reductions using similar control strategies.

While this new "anti-noise" approach has only been analytically studied and proposed to-date, this paper serves, as a first of its kind, to highlight in-plane, low frequency noise reduction possibilities based on acoustic measurement obtained from a recent joint DARPA/Boeing/NASA/Army test[8] completed in April 2008 in the Air Force's National Full-Scale Aerodynamic Complex's 40- by 80-ft anechoic wind tunnel at Moffett Field, California. Of primary interest are results demonstrating the potential of using the Boeing-SMART active flap rotor to mitigate low frequency sounds radiating from near in-plane of the rotor. The extent of noise reduction will be reported in this paper as a function of single-harmonic active flap inputs (amplitude, frequency and phase). Significance of these findings on perceived aural detectability and their implications/limitations on platform applicability will also be discussed.

IN-PLANE, LOW FREQUENCY NOISE SOURCES & REDUCTION STRATEGY

Low frequency rotor harmonic noise originates from several different source mechanisms[9]. As depicted in Figure 1a, one of these mechanisms is attributed to the displacement of surrounding fluid medium due to blade motion. As the blade moves in space, fluid particles in the medium are "pushed" by the moving blade surface causing acoustic waves to be radiated. This mechanism, first studied by Deming[10], is known as the "thickness" or monopole noise

Presented at the American Helicopter Society 65th Annual Forum, Grapevine, Texas, May 27-29, 2009.

and presents itself as a large negative peak pressure known to be a strong function of the advancing tip Mach number and geometry of the airfoil. Subsequent studies have shown that at sufficiently high enough advancing tip Mach numbers, delocalized (weak) shock-fronts are formed at the tips of the rotor blades, resulting in a nonlinear quadrupole phenomenon typically referred to as the "High-Speed Impulsive (HSI)" noise[9]. While HSI noise can be domineering when it occurs, most helicopters today are designed to avoid operating in this region. Therefore, it is not considered in this present study.

The surface pressure distribution around the airfoil due to a lifting rotor also contributes to the sound radiation field. In the absence of strong blade-vortex interaction[9], the resulting low frequency noise radiation is often referred to as steady loading noise[11] due to the inherent (steady) aerodynamic forces necessary to sustain flight. Conveniently, this mechanism can be decomposed into the out-of-plane loading (or the thrust) component and the in-plane loading (torque) component, with respect to the tip-path-plane of the rotor, as shown in Figure 1a. At nominal rotor operating conditions, the out-of-plane loading component is typically dictated by large aerodynamic force values associated with the rotor blade lift. On the other hand, the in-plane loading component results from the vectorial sum of lift and non-viscous drag, and is usually much smaller in magnitude than its out-of-plane counterpart. Over the course of blade rotation and motion, these aerodynamic forces "pound" on the medium and exert their influence on the surrounding fluid to create pressure waves that are radiated into the far-field as noise.

The net noise radiation is the linear sum of all the effects stated above and can be mathematically represented by the well-known Farassat's Formulation 1A (Eqn. 1) for far-field noise radiation[12]. In this formulation, it is assumed that the rotor is operating below the delocalization Mach number and that contributions from the nonlinear quadrupole field are small. At low rotational Mach numbers, it is also often assumed that the surface pressures, at each span station, can be integrated along the chordwise direction and be represented by a spanwise line of rotating point forces. This compact acoustic source approximation is valid when the wavelength of the radiated sound of interest is much larger that the characteristic dimension of the source (blade chord) - a valid approximation here since we are only interested in long-wavelength, low frequency sound in this paper.

$$p'(\vec{x},t) = \int_{f=0}\left[\frac{\rho_o \dot{v}_n}{4\pi \cdot r \cdot (1-M_r)^2}\right]_{ret} dS \quad (Thickness) + \int_{f=0}\left[\frac{\dot{\ell}_i \hat{r}_i}{4\pi c_o \cdot r \cdot (1-M_r)^2}\right]_{ret} dS \quad (Loading) \qquad \text{(Eqn. 1)}$$

Note that Eqn. (1) is in the strictest sense a nonlinear integral equation that requires adding the contributions from all the discretized blade surface elements (of area dS) prescribed on a blade surface, $f = 0$. Often, the right-hand side integrals are assumed to be bounded and finite and basically independent of the left-hand side. The first right-hand side integral illustrates the thickness noise expression as a function of the surface velocity field normal to the blade (v_n). The second term shows the loading noise as a function of the chordwise compact airload vector due solely to the surface pressure (l_i). It contains both out-of-plane component in the z-direction and in-plane component in the x-y plane. In both terms, acoustic radiation is fundamentally governed by the time rate-of-change of the controlling factors. Also, the source term integrands are weighted by the (1-M_r) Doppler factor and are also attenuated by the source-to-observer distance (r). The notation (c_o) denotes the speed of sound of the medium. According to Eqn. (1), the radiated low frequency noise is simply a summation of the thickness and loading source terms taken at each retarded (source) time and correctly propagated and summed at the observer location (x) and time (t).

The nature and complexity of the source integrands render each mechanism's noise radiation directivity to be markedly different from each other. Figure 1b illustrates the far-field noise radiation patterns of the different mechanisms based on predicted values obtained from Eqn. (1) for a typical helicopter at moderate-airspeed level flight cruise. The patterns are shown with normalized noise amplitude (based on the maximum level of each mechanism) at different observer elevation angle positions surrounding the rotor. In general, noise radiated forward of the rotor tends to be greater than noise radiated towards the rear due to Doppler amplification and higher advancing side tip Mach number. It is also evident that different observer positions receive different composition of sound. At positions near in-plane and forward of the rotor, the noise received is primarily due to thickness and in-plane loading mechanisms. This region is confined to about ±30° from the plane of the rotor. On the other hand, the rotor thrust mechanism (out of-plane loading) dominates at locations out-of-plane. These observations are representative of typical lifting-rotor systems and hold true for most conventional single-rotor helicopters.

The presence of both a thickness source term and an in-plane loading term in the in-plane acoustic signature offers an interesting potential for noise cancellation. As discussed before, the two mechanisms originated from very different circumstances and can be treated as two independent, separate source events – thickness noise being solely due to fluid displacement associated with blade motion and geometry, whereas in-plane loading noise is a by-product of the surface pressure acting in the direction near in-plane of the rotor. The two mechanisms are, to first order, un-coupled and have no causality relationships

Because the directivity of the in-plane loading noise nearly matches the directivity characteristics of thickness noise near in-plane of the rotor (Figure 1b), there is a possibility of altering blade airload to generate an in-plane loading noise profile that would negate or reduce the thickness noise pulse (Figure 2). Such an "anti-noise" profile must be of approximately the same shape and magnitude, but opposite in sign. Because most of the thickness noise energy resides in its strong negative peak, it implies that the resulting in-plane loading noise profile must contain a strong positive peak, and must be timed (phased) properly so that the peaks coincide to enable effective cancellation. As shown in a previous study[2], achieving this "anti-noise" profile requires an increase in the in-plane loading as the blade approaches the advancing side near 90° blade azimuth. This result is consistent with findings reported in Reference 7 – which illustrated that an increase in (in-plane) blade loading must be sustained throughout a range ±20° blade azimuth to attain a reasonable "anti-noise" profile that can properly negate the steady thickness noise pulse.

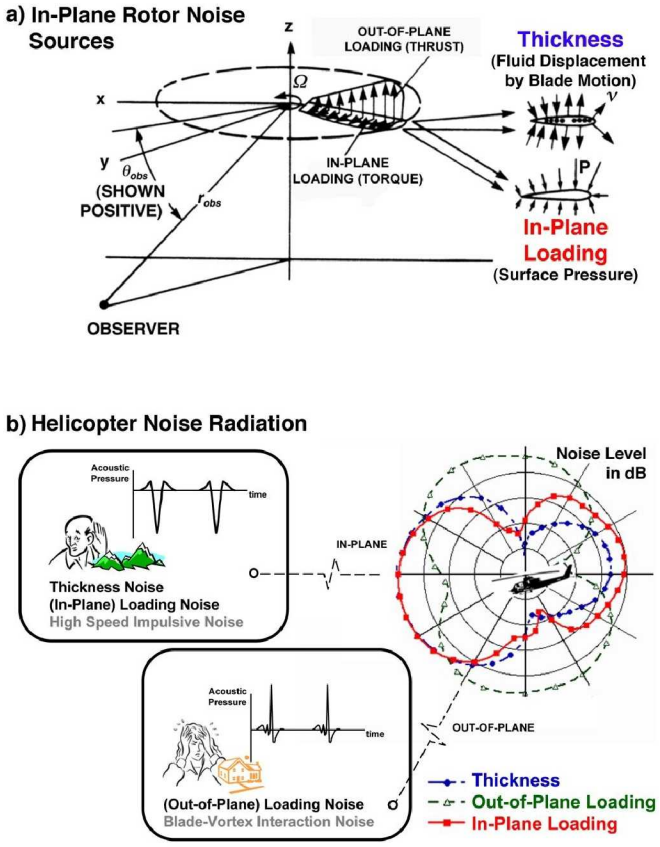

Figure 1. Helicopter noise radiation: a) source components, b) directivity characteristics

Based on these requirements, use of state-of-the-art active controls is deemed a good candidate for realizing such a goal. In most cases, these active control devices are embedded on the blade and/or the hub to enable temporal control of blade structural dynamics and local aerodynamic properties. Additionally, from a noise perspective, these "on-blade" controls are more efficient than conventional active noise control (e.g. fuselage-mounted speaker arrays) in generating the required "anti-noise" pulse due to strong Doppler amplification resulting from high Mach number conditions near the blade tip.

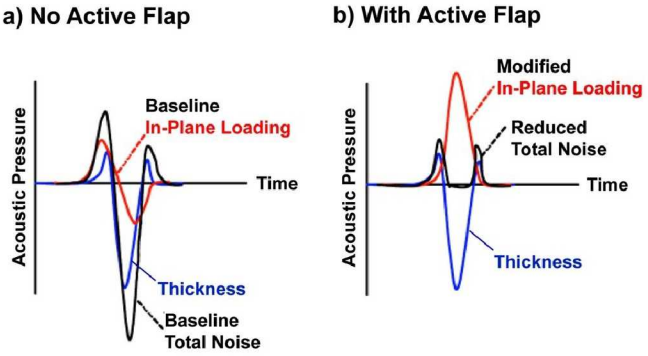

Figure 2. In-plane noise radiation: a) baseline, b) partial cancellation with modified in-plane loading noise

BOEING SMART ROTOR TESTING

An opportunity arose in the early part of 2008 to validate the in-plane noise reduction strategy. Under a joint DARPA/NASA-funded program, Boeing and a team from Air Force, NASA, Army, Massachusetts Institute of Technology, University of California at Los Angeles, and University of Maryland completed a wind-tunnel test of the smart material actuated rotor technology (SMART) rotor in the 40- by 80-foot wind-tunnel of the National Full-Scale Aerodynamic Complex (NFAC) at NASA Ames Research Center. The eleven-week wind tunnel test program[8] evaluated the forward flight characteristics of a full-scale active-flap rotor and quantified the effects of open- and closed-loop active-flap control on rotor loads, noise, and performance. The test demonstrated "on-blade" smart material control of flaps on a full-scale rotor for the first time in a wind tunnel - with effectiveness and reliability of the flap actuation system successfully demonstrated in more than 60 hours of wind tunnel testing.

Rotor Hardware

The SMART rotor (Figure 3) is a 34-ft diameter, full-scale, bearingless, five-bladed main rotor modified from existing MD900 Explorer rotor system. Each blade consists of HH-10 airfoil sections inboard and HH-06 airfoil sections outboard, with a linear twist of –10 degrees. The blade tip has a parabolic leading edge sweep (22 degrees at the tip) and a 2:1 taper ratio. Nominal rotation speed of the rotor is 392 RPM producing a tip speed of 695 ft/sec. At 5,800 lb thrust, the rotor thrust coefficient normalized by rotor solidity is 0.075 at sea level standard conditions.

Each blade contains an embedded piezoelectric actuator designed to drive a 20% span trailing-edge flap at frequencies from two-per-revs (2P) up to six-per-revs (6P), with as much as 4 degrees amplitude authority, depending on the harmonic frequency. Inputs to the five blades are phased azimuthally such that each flap receives the same command at a given azimuth. Equation 2 shows the mathematical representation of a single-harmonically driven flap with deflection angle (δ_f) prescribed as a function of the blade azimuth (ψ), active flap amplitude (A_f), normalized harmonic frequency (H_f) and phase (ϕ_f). Positive deflection angles relate to flap down positions. For the rest of this paper, active flap settings will be described in a three-parameter form, $A_f/H_f \bullet P/\phi_f$ – where A_f and H_f are expressed in degrees and H_f is the normalized harmonic frequency expressed as integer multiples of the rotation frequency.

$$\delta_f = A_f \cdot \sin(H_f \psi + \phi_f) \qquad \text{(Eqn. 2)}$$

Rotor Characteristics

Rotor Blade	Modified MD900
Hub Type	Bearingless
No. of Blades	5
Blade Radius	203.1 inches
Rotor Speed	392 RPM
Tip Chord	10 inches
Airfoil	HH-10, HH-06
Twist	10 deg.

Trailing-Edge Flap Data

Radial Station	150 - 186 inches
Length	36 inches
Chord	3.5 inches
Hinge Location	75% Chord
Max. Flap Angle	± 6 deg.

Figure 3. Boeing-SMART rotor with active trailing-edge flap.

Instrumentation

The Boeing-SMART rotor was supported on top of the Large Scale Dynamic Rig (LSDR) when installed in the NFAC 40- by 80-ft test section (Figure 4a). The LSDR consists of an upper and lower housing connected by a vertical stand strut. In the upper housing, the rotor hub is connected to a static mast, which was mounted to a five-component rotor balance. The static mast encloses the rotating drive shaft that transfers torque directly to the rotor hub. In addition, the upper fairing also encloses the balance housing and the hydraulic servo-actuators for the rotor/active flap control system. A vertical stand strut connects the upper balance housing to the lower housing that encloses the transmission and a 1,500-hp General Electric motor. The LSDR was mounted in the wind tunnel on a three-strut support system placing the rotor hub 23.7 ft above the tunnel floor at zero degree shaft tilt.

For acoustic measurement, a series of microphones was strategically placed around the model to capture rotor noise sources of interest (Figure 4a). These microphones were grouped into: a) out-of-plane fixed microphones (M1 and M4) to correlate to microphones used previously in the MDART test[13], b), traverse microphones (M5 through M12) that can be moved along guided rails for blade-vortex interaction noise mapping and c) in-plane microphones (M13, M15 and M14) for low frequency, in-plane rotor noise measurement. Microphones M13, M15 and M14 were mounted on tower struts to be near in-plane of the rotor (approximately 10 degrees below wind tunnel horizon). These microphones were also intentionally positioned along a straight line originating from the advancing blade tip to the tunnel centerline (Figure 4b) to enable near-field/far-field correlations of in-plane rotor noise. With the exception of M14, all microphones are located within the acoustically-treated portion of the 40- by 80-ft test section. Summaries of the microphone positions, relative to both the rotor hub and to the advancing blade tip, are illustrated in Table 1a and 1b respectively.

a) SMART Rotor Testing

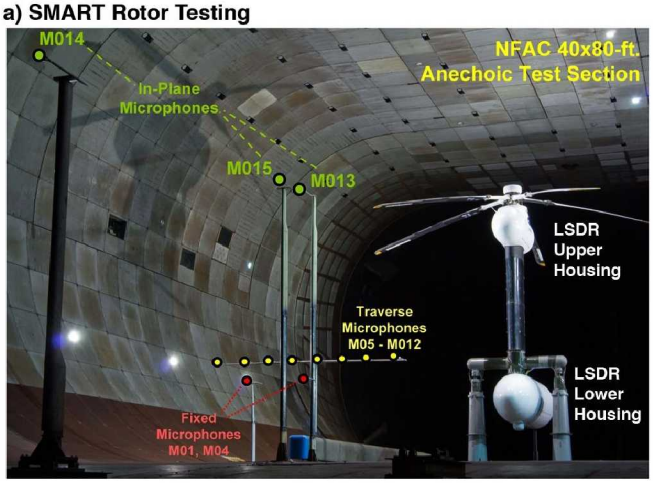

b) Microphone Layout (Top View)

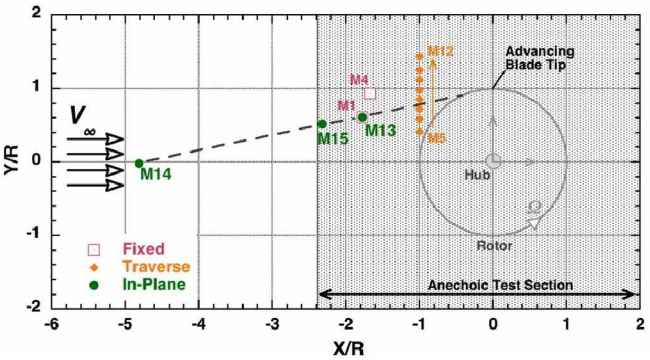

Figure 4. Test setup: a) Boeing-SMART rotor installation in wind tunnel, b) microphone layout.

Instrumentation-grade 1/2-inch free-field condenser microphones (G.R.A.S. Type 40AC) with nose cone fairings were used in the acoustic measurement. Microphone signals were pre-amplified at the source to minimize signal loss over the long wiring runs leading to a junction box housed below the test section - upon which the signals are tee-ed off to both an acoustic monitoring station and to the data acquisition console. Microphone gains were adjusted at the monitoring station on a per-test point, per-channel basis to maximize signal-to-noise ratio. In addition to the microphone signals, encoders on the rotor shaft provided a one-per-rev trigger signal, as well as a 256-pre-rev and a 2048-per-rev sampling clock.

Table 1a. Hub-centered Microphone Positions

Mic. No.	XH, ft	YH, ft	ZH, ft	rH,ft	rH/R	ΨH, deg.	ΘH, deg.	
M1	-29.67	10.27	-17.94	36.16	2.14	160.9	-29.7	Fixed
M4	-27.92	15.59	-17.87	36.63	2.16	150.8	-29.2	
M5	-16.73	6.97	-15.13	23.61	1.39	157.4	-39.9	Traverse (ASA -200)
M6	-16.73	9.79	-15.13	24.59	1.45	149.7	-38.0	
M7	-16.73	12.02	-15.13	25.56	1.51	144.3	-36.3	
M8	-16.73	14.17	-15.13	26.64	1.57	139.7	-34.6	
M9	-16.73	16.42	-15.13	27.90	1.65	135.5	-32.8	
M10	-16.73	18.67	-15.13	29.28	1.73	131.9	-31.1	
M11	-16.73	20.90	-15.13	30.75	1.82	128.7	-29.5	
M12	-16.73	23.92	-15.13	32.88	1.94	125.0	-27.4	
M13	-29.67	10.27	-5.34	31.85	1.88	160.9	-9.7	In-Plane
M15	-38.77	8.73	-7.13	40.38	2.39	167.3	-10.2	
M14	-80.36	-0.33	-14.84	81.72	4.83	180.2	-10.5	

XH - Positive towards aft, YH - Positive towards starboard, ZH - Positive up

Table 1b. Advancing Blade Tip-centered Microphone Positions

Mic. No.	XA, ft	YA, ft	ZA, ft	rA,ft	rA/R	ΨA, deg.	ΘA, deg.	
M1	-29.67	-6.43	-17.94	35.26	2.11	192.2	-30.6	Fixed
M4	-27.92	-1.11	-17.87	33.17	1.99	182.3	-32.6	
M5	-16.73	-9.73	-15.13	24.57	1.47	210.2	-38.0	Traverse (ASA -200)
M6	-16.73	-6.91	-15.13	23.59	1.41	202.4	-39.9	
M7	-16.73	-4.68	-15.13	23.04	1.38	195.6	-41.1	
M8	-16.73	-2.53	-15.13	22.70	1.36	188.6	-41.8	
M9	-16.73	-0.28	-15.13	22.56	1.35	181.0	-42.1	
M10	-16.73	1.97	-15.13	22.64	1.36	173.3	-41.9	
M11	-16.73	4.20	-15.13	22.94	1.37	165.9	-41.3	
M12	-16.73	7.22	-15.13	23.68	1.42	156.7	-39.7	
M13	-29.67	-6.43	-5.34	30.82	1.85	192.2	-10.0	In-Plane
M15	-38.77	-7.97	-7.13	40.22	2.41	191.6	-10.2	
M14	-80.36	-17.03	-14.84	83.47	5.00	192.0	-10.2	

XA - Positive towards aft, YA - Positive towards starboard, ZA - Positive up

Data Acquisition

With the exception of some monitoring parameters used for Boeing's active flap control system, most data from the LSDR, wind tunnel and microphones were recorded on the NFAC's multi-channel data acquisition system. For each test point, sixty-four revolutions of data (approximately 9.75 secs) were collected to enable time-domain averaging on a rotor revolution basis. This order-tracking procedure isolates harmonic contents pertaining only to the rotation rate of the rotor, and suppresses all other un-wanted frequency contents, to achieve superior signal-to-noise ratio. All channels, but the acoustic measurement, were sampled at 256 samples per revolution using the sampling clock from the rotor encoder. Acoustics data were separately sampled at a higher rate – at 2048 samples per revolution, to capture the mid-to-high frequencies associated with human audible range.

Acoustics Test Matrix

While the scope of the Boeing-SMART rotor test embodies a wide variety of flight conditions, in-plane rotor noise reduction was investigated only at a single operating condition corresponding to 123 knots level flight cruise (advance ratio of 0.30). At this condition, the nominal shaft tilt (un-corrected) was –9.11 degrees, with an advancing tip Mach number of 0.81 and a rotor thrust-to-solidity ratio of 0.075. Effects of active flap deployment were systematically studied via phase and amplitude sweeps at various active flap frequencies. A summary of the test points, used in this paper, and their corresponding operating conditions, is illustrated in Table 2. For all these cases, the rotor was first trimmed to zero blade-flapping moment prior to active flap deployment.

Table 2. Acoustics Test Matrix

	Active Flap			Wind Tunnel Condition						Data Tracking		
	Af, deg.	Hf, P	φf, deg.	Tunnel Velocity, kt	Uncorr. Shaft Tilt, deg.	Advance Ratio	Rotational Tip Mach Number	Advancing Tip Mach Number	Thrust-to-Solidity Ratio	Boeing Event No.	NFAC Run No.	NFAC Point No.
Baseline				124.8	-9.11	0.299	0.622	0.808	0.07493	39.08300	57	68
2P Phase Sweep	1.5	2	0	124.8	-9.11	0.299	0.623	0.809	0.07427	39.07000	57	55
	1.5	2	30	124.8		0.299	0.623	0.809	0.07518	39.07100	57	56
	1.5	2	60	124.7		0.298	0.623	0.809	0.07605	39.07200	57	57
	1.5	2	90	124.9		0.299	0.623	0.809	0.07535	39.07300	57	58
	1.5	2	120	124.6		0.298	0.623	0.808	0.07492	39.07400	57	59
	1.5	2	150	124.7		0.298	0.623	0.809	0.07421	39.07500	57	60
	1.5	2	180	124.6		0.298	0.623	0.809	0.07455	39.07600	57	61
	1.5	2	210	124.6		0.298	0.623	0.809	0.07493	39.07700	57	62
	1.5	2	240	124.9		0.299	0.623	0.808	0.07621	39.07800	57	63
	1.5	2	270	124.9		0.299	0.622	0.808	0.07544	39.07900	57	64
	1.5	2	300	124.5		0.298	0.623	0.808	0.07651	39.08000	57	65
	1.5	2	330	124.8		0.299	0.623	0.808	0.07605	39.08100	57	66
	1.5	2	360	124.8		0.299	0.623	0.808	0.07599	39.08200	57	67
2P Amplitude Sweep	1	2	0	124.1	-9.11	0.298	0.623	0.810	0.07554	38.02700	55	27
	1.5	2	0	124.1		0.299	0.622	0.808	0.07344	38.02800	55	25
	2	2	0	124.3		0.299	0.623	0.809	0.07440	38.02600	55	26
3P Phase Sweep	1.5	3	0	124.0	-9.11	0.300	0.623	0.810	0.07571	33.03100	46	29
	1.5	3	30	123.6		0.299	0.623	0.809	0.07487	33.03200	46	30
	1.5	3	60	123.4		0.299	0.623	0.809	0.07441	33.03300	46	31
	1.5	3	90	123.9		0.300	0.623	0.809	0.07425	33.03400	46	32
	1.5	3	120	123.6		0.299	0.623	0.809	0.07353	33.03500	46	33
	1.5	3	150	123.1		0.298	0.623	0.809	0.07433	33.03600	46	34
	1.5	3	180	123.4		0.299	0.623	0.809	0.07605	33.03700	46	35
	1.5	3	210	123.8		0.300	0.623	0.810	0.07443	33.03800	46	36
	1.5	3	240	123.7		0.299	0.623	0.808	0.07465	33.03900	46	37
	1.5	3	250	123.4		0.298	0.623	0.808	0.07472	33.04700	46	45
	1.5	3	270	123.4		0.299	0.623	0.809	0.07505	33.04000	46	38
	1.5	3	300	123.3		0.298	0.623	0.809	0.07572	33.04100	46	39
	1.5	3	330	123.4		0.299	0.623	0.809	0.07600	33.04200	46	40
	1.5	3	360	123.5		0.299	0.623	0.809	0.07724	33.04300	46	41
3P Amplitude Sweep	1	3	250	124.2	-9.11	0.299	0.623	0.810	0.07517	38.02800	55	28
	1.5	3	250	123.4		0.298	0.623	0.808	0.07472	33.04700	46	45
	2	3	250	123.5		0.299	0.623	0.808	0.07319	33.04800	46	46
4P Phase Sweep	1	4	0	123.4	-9.11	0.300	0.623	0.809	0.07554	37.06500	54	36
	1	4	30	123.4		0.300	0.623	0.809	0.07588	37.06600	54	37
	1	4	60	123.1		0.298	0.623	0.809	0.07930	37.06700	54	38
	1	4	90	123.6		0.300	0.623	0.809	0.07839	37.06800	54	39
	1	4	120	122.8		0.298	0.623	0.809	0.07756	37.06900	54	40
	1	4	150	123.2		0.299	0.623	0.809	0.07788	37.07000	54	41
	1	4	180	123.2		0.299	0.623	0.809	0.07802	37.07100	54	42
	1	4	210	123.7		0.300	0.623	0.810	0.07578	37.07200	54	43
	1	4	240	123.4		0.299	0.623	0.809	0.07719	37.07300	54	44
	1	4	270	123.3		0.299	0.623	0.809	0.07791	37.07400	54	45
	1	4	300	123.5		0.300	0.623	0.810	0.07748	37.07500	54	46
	1	4	330	123.5		0.300	0.623	0.809	0.07854	37.07600	54	47
	1	4	360	123.2		0.299	0.623	0.809	0.07882	37.07700	54	48
4P Amplitude Sweep	0.7	4	180	124.5	-9.11	0.299	0.623	0.809	0.07748	38.02100	55	21
	1	4	180	123.9		0.299	0.623	0.809	0.07643	38.01900	55	19
	1.3	4	180	124.0		0.299	0.623	0.810	0.07685	38.02000	55	20

LOW FREQUENCY NOISE MEASUREMENT

Prior to the beginning of the Boeing-SMART rotor test, it was deemed necessary to re-examine the acoustic quality of low frequency sound measurement in the 40- by 80-ft test section. Recent modification of the 40- by 80-ft test section

walls, in 1997, with 42-inch deep acoustic liners reportedly improved and expanded aeroacoustics testing capabilities[14]. Subsequent post-mod calibration[15] reported superior sound absorption capabilities of 94% or more between 100 Hz and 2,500 Hz at most places in the test section. Unfortunately the frequency range examined did not extend to the lower frequency regimes that are of interest to the current Boeing-SMART rotor test – namely for the first three blade-passing harmonic tones at 32.7 Hz, 65.4 Hz and 98.1 Hz.

A sound quality assessment was initiated in early January 2008 to evaluate how these low frequency harmonic tones propagate in an empty 40- by 80-ft test section under static, no-wind conditions. Using a calibrated sub-woofer, positioned at the advancing blade tip of the Boeing-SMART rotor, acoustic measurements were obtained along a straight line that extended from the advancing blade tip position to the centerline of the tunnel (Figure 4b). Audio tracks generated by a Matlab-based sound engine were played through the sub-woofer to simulate the dominant low frequency noise sources. This included harmonic pure tones corresponding to each of the blade-passing frequencies of the Boeing-SMART rotor and a mixed-harmonic audio track that combined multiple low frequency tones (first six blade-passing harmonics) to mimic helicopter noise. Obtaining noise measurement, at increasing distances from the sub-woofer source, provide valuable insights to the quality of sound measurement in the enclosed test section. If the acoustically-treated surfaces are truly anechoic, noise measurements must follow an inverse-distance decay law (i.e. 6 dB drop-off per doubling of distance) observed in a free-field environment. Any deviations from this free-field trend suggest the presence of facility-induced effects that leads to inaccurate representation of the source noise.

A summary of the results obtained from this sound quality assessment effort is illustrated in Figure 5. Relative sound pressure levels, at different frequencies, are plotted as a function of increasing distance from the sub-woofer sound source. Results for frequencies greater than 100 Hz appears to be consistent with findings reported in Reference 15. Tonal sound decay with distance generally followed the 6 dB drop-off line, but showed oscillations of up to 3 dB within 40 feet from the sub-woofer source. As stated in Reference 15, these fluctuations were attributed to non-uniform wall sound absorption characteristics in various parts of the test section. At distances beyond 40 feet (outside of the acoustically-treated portion of the test section), much larger oscillations on the order of 6 dB or greater were observed.

Similar trends were shown for the simulated helicopter noise signature with mixed-harmonic tones, but with smaller oscillation amplitudes up to 50 feet. These results imply that low frequency sound measurement at microphones M13 and M15 have relatively subdued facility effects and suggest the likelihood of adequate source noise representation at these locations (within an error band of ±2 dB). Unfortunately, as shown in Figure 5, this does not hold true for the furthest microphone (M14), located 80 feet away outside of the acoustically-lined portion of the test section.

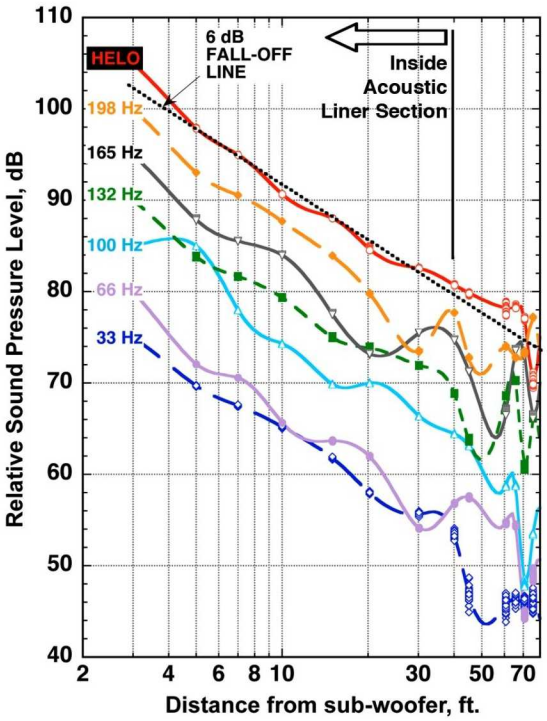

Figure 5. Low frequency sound assessment of the 40- by 80-ft test section.

Another factor that raises sound quality measurement concerns is the amount of ambient noise level present during "wind-on" conditions. Typically, ambient noise is dictated by the facility's fan drive system[16], but can include tonal/broadband sounds generated by hydraulic systems and flow-induced sounds from rotor test stand, wind tunnel surface or acoustics apparatus, such as microphone strut and/or microphone body. For all test data illustrated in this paper, the NFAC's variable-pitch fan-drive system operated at Induction Frequency Changer (IFC) mode with a fan speed of 115 RPM. Corresponding ambient noise levels measured at the three in-plane microphones (M13, M15 and M14) are indicated by the green lines in Figure 6. These ambient noise levels were obtained at 123 knots wind speed, with a rotating bare hub (without blades) operating at the nominal rotor RPM of 392. Compared to the Boeing-SMART rotor in baseline configuration (without active flap deployment), good signal-to-noise ratios of 18 dB or greater were observed for the two closer microphones M13 and M15. As shown in Figure 6c, the far-away microphone M14 did not fair as well at certain blade-passing harmonics. It is also shown that microphone M14 cannot replicate the source noise characteristics of the rotor, and will therefore be excluded from future discussions.

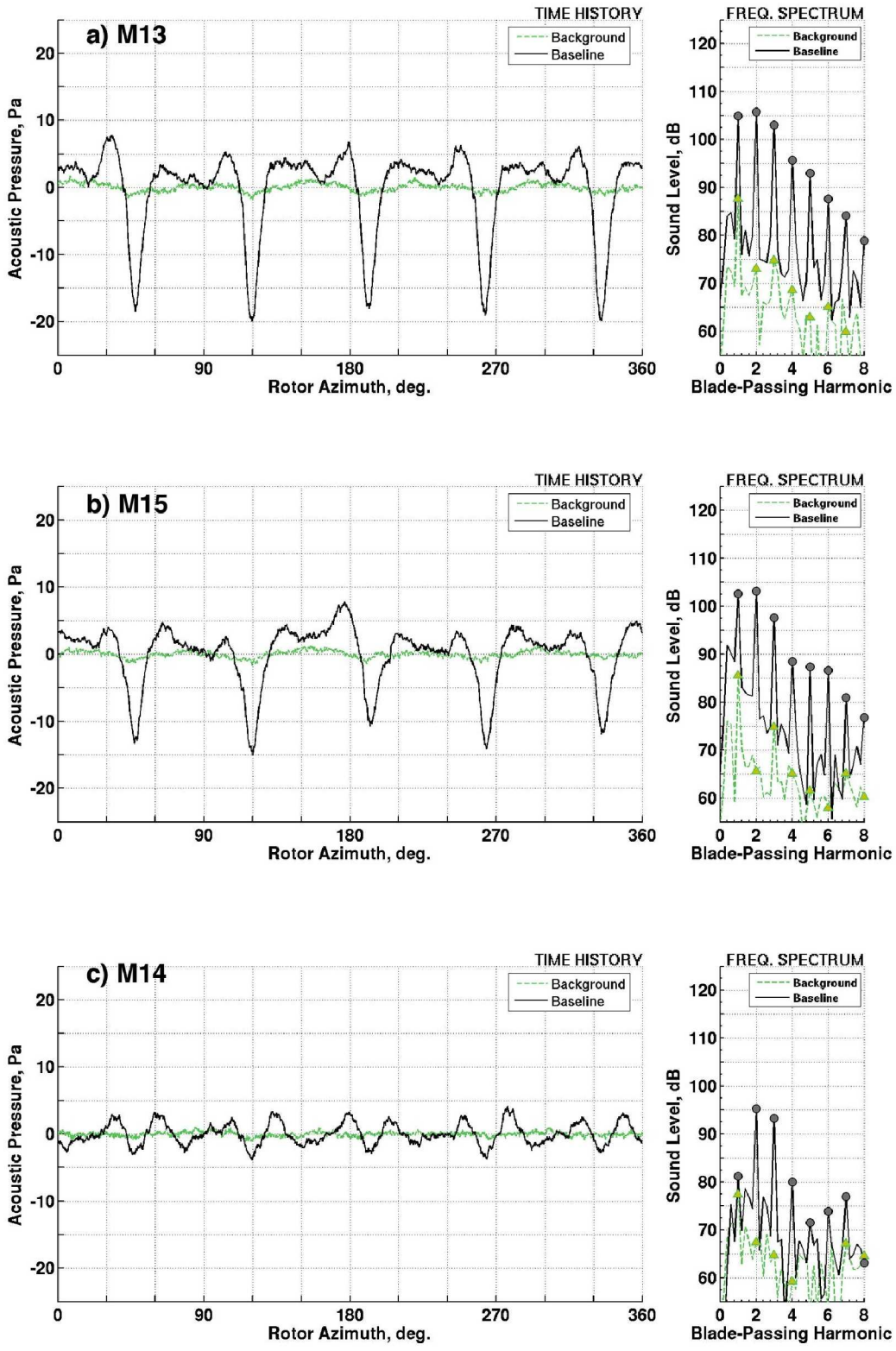

Figure 6. Rotor noise signal and ambient noise (64 revolutions) averaged time histories and corresponding frequency spectra at $\mu = 0.30$ for: a) M13, b) M15,, c) M14.

Given the limitations of the facility, proximity of the installed microphones to the rotor is also a source of concern. Housing the full-scale Boeing-SMART rotor in the 40- by 80-ft test section, with constraints imposed on microphones to be installed within the acoustically-treated section of the tunnel, challenges the ability to make accurate measurement representative of far-field external rotor noise radiation. Classical aeroacoustics theory stipulates that true far-field noise decays in an inversely-proportional manner with distance from its source. This implies that any distance-weighted acoustic metric must becomes invariant (with distance) in the far-field. Results in Figure 7 for microphones M13 and M15, at baseline rotor configuration, demonstrate that this is indeed the case. Even though these microphones are no more than $3R$ away from the advancing blade tip, distance-weighted acoustic time histories and spectral band levels showed similar amplitudes and features between the two microphones. Some discrepancies observed at the fourth and fifth blade-passing harmonics were attributed to increased amount of facility wall-induced effects at microphone M15.

LOW FREQUENCY NOISE PREDICTIONS

In additional to noise data from wind tunnel measurement, predictions of low frequency sound for the Boeing-SMART the rotor will be presented in this paper. Rotor noise predictions are derived from blade geometry and predicted blade airload properties. The latter is obtained from comprehensive rotor analysis CAMRAD-II[17] using analytical modeling of the blade structural properties, rotor wake geometry, and local unsteady blade aerodynamics. Within the analysis, blade modeling is based on finite nonlinear beam elements, where each blade is discretized into a series of nonlinear beam elements (finite element). Each beam element is represented by a full range of blade motions, including axial, lead-lag, flapping and torsional blade dynamics. Trailing-edge flap is locally accounted for via span-wise changes in the blade stiffness and mass properties associated with the hinged flap. A non-uniform inflow model coupled to a free wake is used to obtain trimmed aerodynamic forces and blade motion solutions at a pre-defined rotor thrust and pitch at zero blade-flapping.

In all ensuing calculations, the rotor blade is modeled using twenty aerodynamic panels on each blade and is evaluated at azimuth intervals of 15°. The panels are more densely distributed at the outboard (tip) region of the rotor blade to accurately simulate the dominant region important for sound radiation. The relatively large time (azimuth) step is found to be adequate for capturing low frequency sounds (up to six blade-passing harmonics) addressed in this paper. Steady airload are computed using C-81 airfoil tables. Unsteady lift and moment in the attached flow are calculated based on compressible thin-airfoil theory. Provisions for modeling trailing-edge flap aerodynamics were incorporated via an extension of the airfoil tables to include flap angle as an input parameter. An empirically-based Mach number correction[18] is recently incorporated to better correlate to measured torsion and flap bending loads. This correction is applied only at the blade tip region (from 74% blade radius to the tip) to account for the effects of compressibility.

PSU-WOPWOP[19] is used to generate acoustics predictions reported in this paper. The code makes use of the blade geometry, and CAMRAD-II-derived blade motion and aerodynamic loading to resolve rotor acoustics radiation in the time domain. The acoustic equation, Farassat's Formulation 1A (Eqn. 1), is implemented in PSU-WOPWOP to relate the afore-mentioned blade geometry and airload properties to acoustic pressures at observers in both the near and the far-field. In this paper, PSU-WOPWOP is configured to simulate a single rotor operation in a steady-state, wind tunnel environment. Only the linear thickness noise source and "on-surface" loading noise source terms are considered.

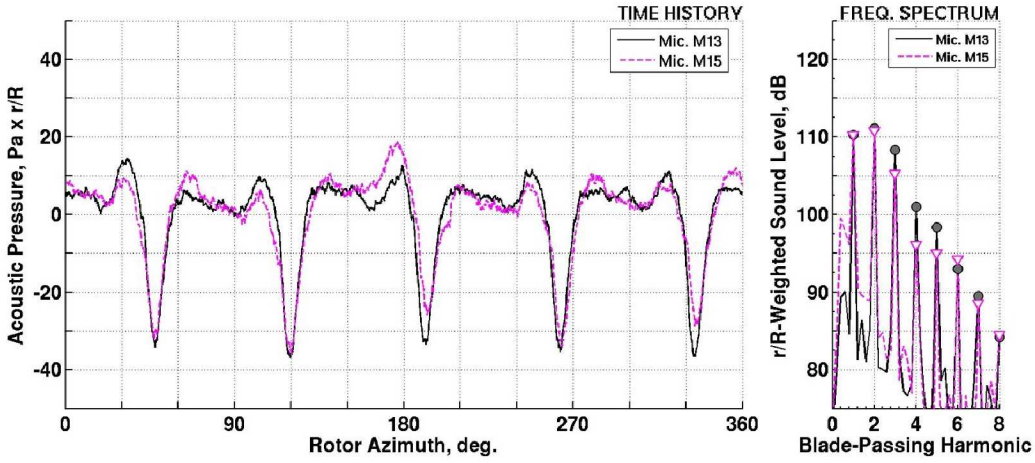

Figure 7. Near-field/far-field comparison of averaged time histories and frequency spectra for microphone M13 and M15.

RESULTS & DISCUSSIONS

The following section reports findings from the Boeing-SMART rotor test during which the active flap was systematically deployed to minimize low frequency, in-plane noise. Results are shown for single harmonic flap actuation schedules, as a function of three active flap parameters: amplitude, frequency and phase, and are compared to baseline (no active flap) configuration, whenever necessary, to assess their potentials for low frequency, in-plane noise mitigation. These results will be reported solely based on microphone M13 measurement, even though similar findings were observed for microphone M15 as well.

Baseline configuration

Figure 8 shows the sixty-four revolution-averaged acoustic time history and frequency spectra (for the first eight blade-passing harmonics) measured at baseline configuration (with no active flap deployment) at microphone M13. Over the course of one rotor revolution from 0° to 360° rotor azimuth, five distinct pulses manifest in the time history – each owing its origin to a different blade on the five-bladed Boeing-SMART rotor system. A large negative pressure peak dominates each pulse. As discussed before, this is primarily attributed to the thickness noise mechanism associated with blade/airfoil geometry rotating at moderate-to-high Mach numbers. Although not explicitly shown, there is a smaller contribution from loading noise mechanism due to in-plane, chord-wise blade forces, that accounts for approximately one-third of the acoustic energy[7] at this advancing tip Mach number.

From the same figure, it is also evident that in-plane noise radiation of the Boeing-SMART rotor is dominated by relatively large pulse-width, hence low frequency, negative thickness noise peaks – with very little mid-to-high frequency content commonly associated with impulsive rotor noise mechanisms, such as blade-vortex interactions. At 109.76 dB, the low frequency sound pressure level (LFSPL) noise metric, which embodies acoustic energy only in the first six blade-passing harmonics, is of comparable magnitude with the full-spectrum energy level depicted by the overall sound pressure level (OASPL). A mid-frequency sound pressure level indicator, which accounts for higher frequencies (sixth blade-passing harmonic and higher), shows a magnitude that is 20 dB smaller. Naturally, this implies that in-plane noise radiation of the Boeing-SMART rotor, at this operating condition, is primarily inundated by lower frequencies associated with lower-order blade-passing harmonic tones.

Predictions from CAMRAD-II/PSU-WOPWOP are shown to be in excellent agreement with measurement. Gross features of the acoustic time history, and in particular, the negative peak pressures, are well simulated for the baseline configuration with no active flap deployment. Predicted spectral band levels show less than 2 dB differences, compared to measured values, for the first eight blade-passing harmonics.

Single harmonic flap input: Phase sweep

Figure 9 illustrates the effects of operating the active flap at two-, three- and four-per-rev (2P, 3P and 4P) separately, as a function of input phase angles depicted on the x-axis. At 2P and 3P settings, the active flap was commanded to deliver a flap deflection of 1.5°; whereas, only a 1.0° flap amplitude was realized at 4P due to high blade loads that exceeded safety load limits. Changes in LFSPL decibel levels at microphone M13 (from baseline value) are plotted on the y-axis with negative decibel numbers indicating reduction in noise levels.

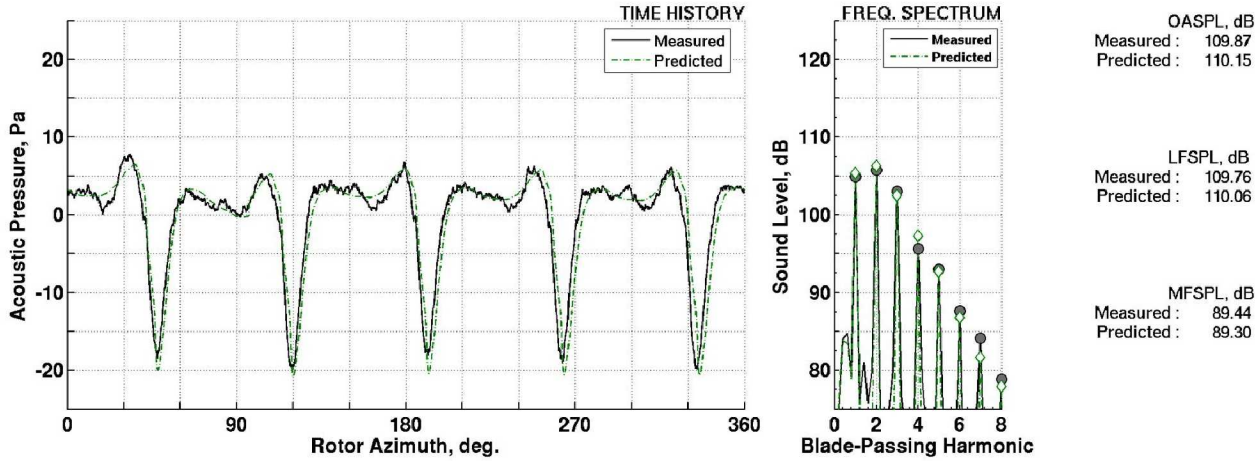

Figure 8. Measured and predicted acoustic time histories and frequency spectra for baseline condition (microphone M13).

Figure 9 reveals that low frequency noise at microphone M12 varies with input phase setting during single harmonic flap actuations. While a majority of these settings increased noise, there were certain phase inputs that resulted in noise reductions. Note that each active flap frequency setting resulted in a somewhat different "best" phase angle that delivered the greatest amount of noise reduction. For 2P flap actuation, this "best" phase angle occurs at 0°, while at 3P, it is shifted to 250°, and eventually becomes 180° at 4P. The amount of reduced low frequency noise is also different at each of these frequencies: with 2.8 dB reduction at 2P, 4.5 dB reduction at 3P and 4.8 dB reduction at 4P. As will be shown in subsequent sections, these "best" phase angle values and their corresponding dB reductions trends are intrinsically related to changes in the blade aerodynamic forces and blade motions/dynamics induced by the sinusoidally-oscillating flap.

Noise predictions for these phase sweep conditions are also shown in Figure 9 to yield favorable comparisons with measured data. The general noise trends are well-captured, with predicted noise reduction amplitudes matching measured values to within ±3 dB. A slight discrepancy in the predicted "best" phase setting is noticed, which amounts to approximately 30° lag in phase for 2P and 4P cases, and about 10° lag at 3P. The reason for this phase lag is unknown, but it would suggests that existing comprehensive rotor analyses may not have sufficient fidelity to capture trailing-edge flap aerodynamics accurately.

Acoustic time histories for these measured and predicted "best" phase conditions are illustrated in Figure 10. Compared to measured baseline noise, operating active flap in these manners clearly suppress the strong negative pressure peaks that set the low frequency sound levels at microphone M13. For 3P and 4P flap settings, the measured negative peak pressures associated with each blade were reduced by almost 50%. Reductions in the measured spectral band levels were also observed, although not uniformly across all blade-passing harmonics. As discussed before, this phenomenon owed its origin to the active flap's ability to alter blade aerodynamics locally on the rotor where the dominant noise source resided. At these "best" phase conditions, an "anti-noise" pulse triggered at the right time was able to partially cancel the negative peak pressure. It is also shown that additional noise was introduced due to the prescribed sinusoidal flap motion that unnecessarily modified blade airloads at other locations on the rotor.

Predicted noise profiles demonstrated good correlation with measured negative peak pressures, in terms of both amplitudes and trends. Results from CAMRAD-II/PSU-WOPWOP were consistent in showing a smaller reduction in negative peak pressures for 2P active flap frequency and larger reductions for 3P and 4P. However, time history predictions in the vicinity of the negative peak pressure seem to deviate in details from measurement. In particular, the predictions indicated presence of additional acoustic pressure fluctuations that resulted in the spectral band levels from the fourth blade-passing harmonics upwards to be increased. This effect was not observed in noise measurement obtained during wind tunnel testing.

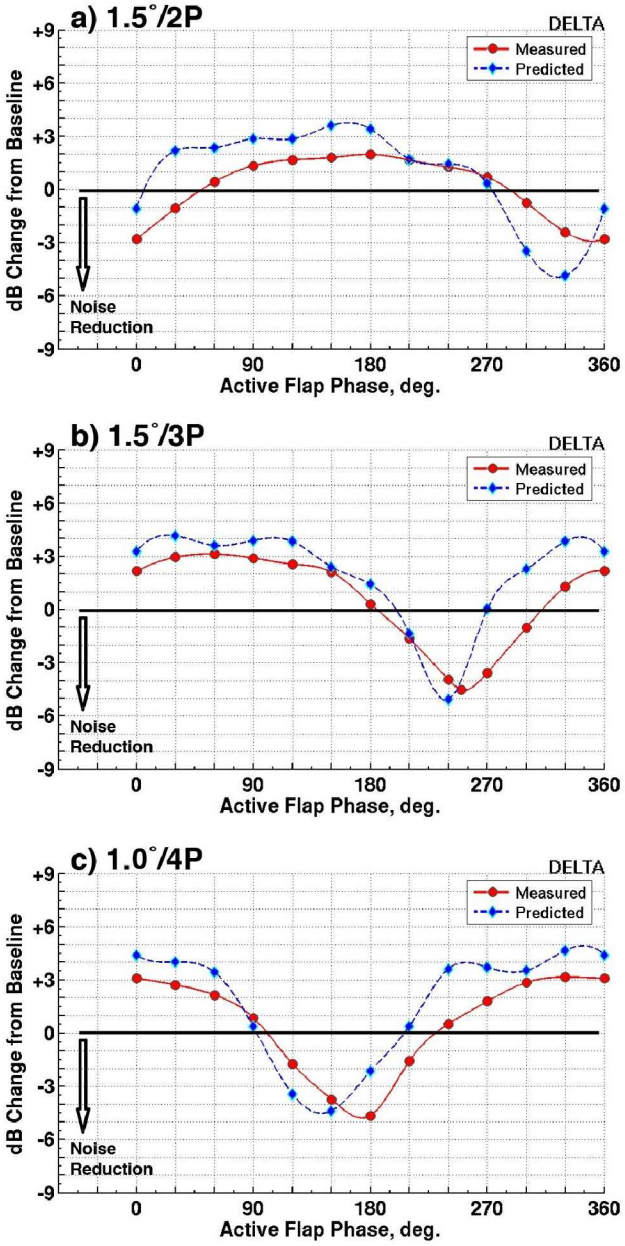

Figure 9. Changes in LFSPL (from baseline) at microphone M13 as a function of active flap phase input: a) 1.5°/2P, b) 1.5°/3P, c) 1.0°/4P.

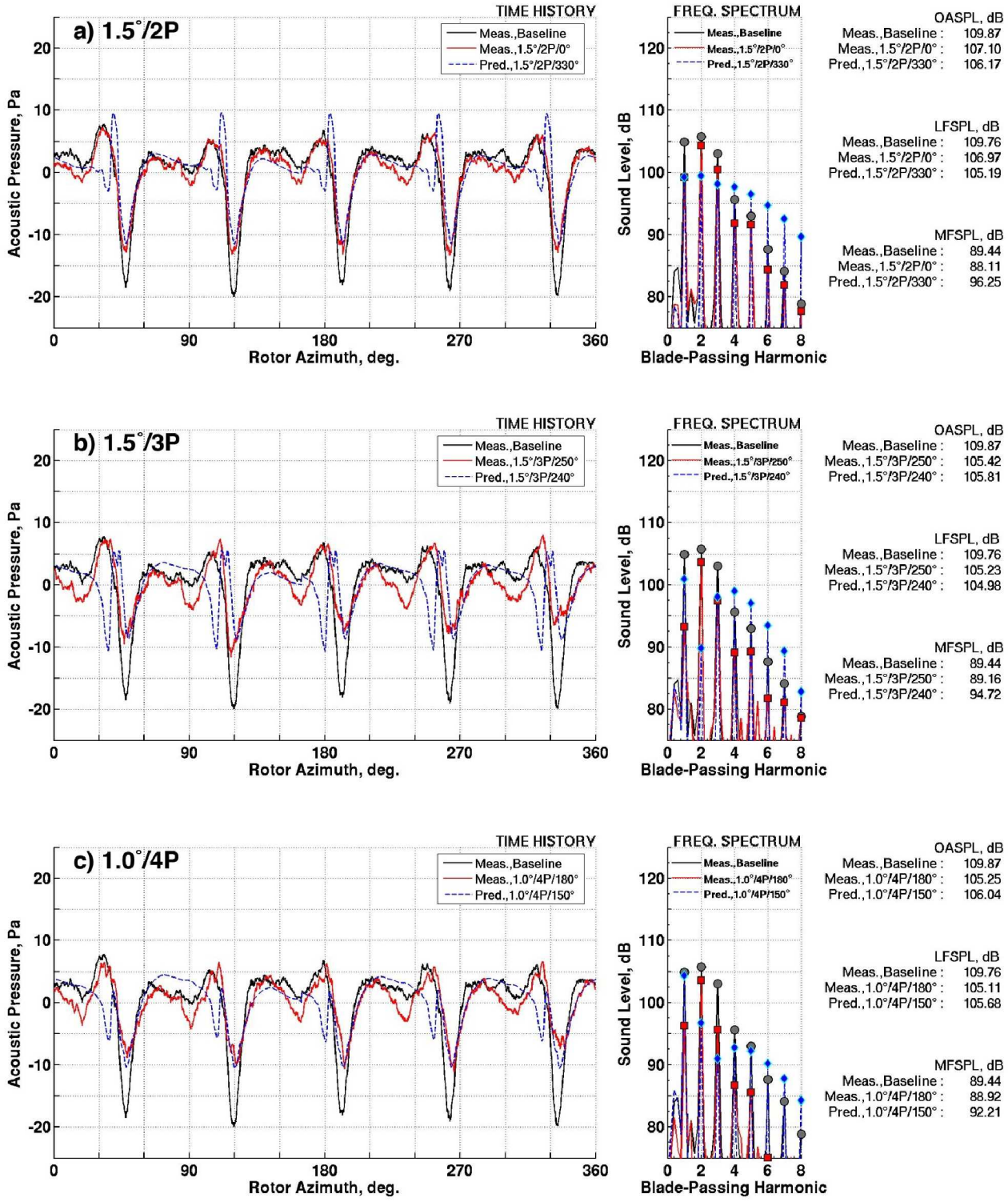

Figure 10. Acoustic time histories and frequency spectra at "best" phase conditions (microphone M13): a) 1.5°/2P, b) 1.5°/3P and c) 1.0°/4P.

The different "best" active flap phase settings at each frequency are governed by flap-induced blade dynamics, and the resulting aerodynamic forces. Figure 11 illustrates measured active flap deflection at blade 1 on the advancing side of the rotor from 0° to 180° blade azimuth, where the bulk of forward, in-plane noise is known to originate from. These flap deflection plots are shown for the different "best" 2P, 3P and 4P phase scenarios, along with blade torsion, flap-wise bending and chord-wise bending time histories at the 82% radial station. For comparison purposes, similar time histories for baseline conditions, and for a "worst" phase setting, typically at 180° out-of-phase, are shown.

The most striking feature in Figure 11 is the presence of a consistent trend that governs when noise reduction occurs. At the advancing tip position around 90° blade azimuth, all the "best" phase scenarios showed decreasing flap deflections with time (azimuth) – signifying that the active flap is moving from a flap down position (positive flap deflection) to a flap up position (negative flap deflection). This is found to be the case for all 2P, 3P and 4P flap actuations. Note that the flap operated in opposite manners for the all the "worst" phase scenarios.

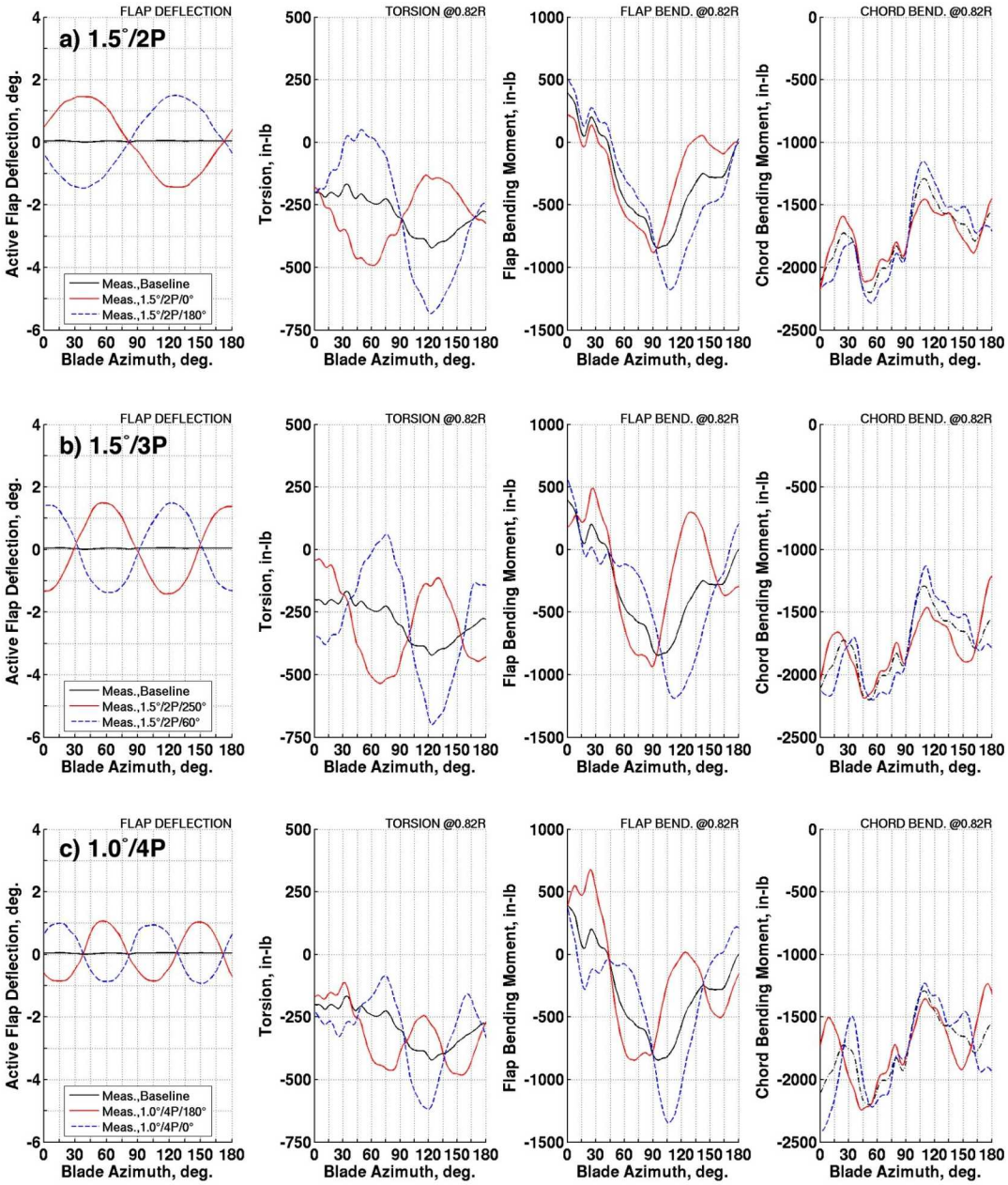

Figure 11. Measured (blade 1) flap deflection and blade dynamics (at 0.82*R*) for "best" and "worst" phase conditions: a) 1.5°/2P, b) 1.5°/3P and c) 1.0°/4P.

Similar observations are identified in measured blade dynamics properties. "Best" noise reduction consistently occurs when blade torsion (positive, pitch-up) increases with blade azimuth on the advancing side of the rotor near 90°, albeit from a highly negative, pitched-down state. Likewise, flap-wise bending moment (positive, flap-up) is always increased at or near 90° blade azimuth, whenever the active flap reduces noise. Compared to baseline, these measurements suggest that the blade tip region must be pitching nose-up and simultaneously be flapping up, to impart favorable noise reduction. The opposite holds true for the "worst" phase scenarios where noise is amplified by deploying the active flaps.

Effects on measured chord-wise bending moments (positive, lag) are less obvious. Compared to baseline, the only visible change is a decrease in chord-wise bending moment (and its rate-of-change) near 90° blade azimuth during "best" phase operations, and, vice-versa, for the "worst" phase. This implies that the blade section experiences a larger chord-wise "drag" force (compared to baseline) during reduced in-plane noise operations – a requirement originally hypothesized in References 2 and 7, and at the beginning of this paper, as a pre-requisite for generating the "anti-noise" pulse to negate in-plane thickness noise.

Lack of blade pressure instrumentation precludes direct quantification of the influence of active flap on blade air-load. However, based on observations stated above, reduced in-plane noise can be attributed to increase in in-plane blade forces (positive towards trailing-edge) on the advancing side of the rotor. This is likely caused by aerodynamic load that were modified by active flap-induced blade torsions and blade flapping motions. As illustrated in Figure 12a, when the blade undergoes a pitch-up and flap-up motion caused by the active flap deflecting upwards, the airfoil at each span-wise station experienced a downward-velocity relative to the medium. This caused the local effective velocity to be angled down relative to the rotor tip-path-plane, and tilted the lift vector backwards towards the trailing-edge. In doing so, the net in-plane force, which is the vectorial sum of both lift and drag component in the tip-path-plane, was increased. On the other hand, a decrease in in-plane force occurred when the effective velocity was angled up due to pitch-down and flap-down motions. The lift vector was subsequently tilted forward which decreased the in-plane force associated with downward deflection of the active flap near the advancing side of the rotor (Figure 12b).

Based on these results for in-plane microphone M13, it is possible to surmise that the "best" phase setting ($\phi_{f,Best}$) is strictly a function of the active flap (single harmonic) frequency, H_f, which can be approximated by,

$$\phi_{f,Best} \approx 180^\circ \cdot \left(1 - H_f/2\right) \qquad \text{(Eqn. 3)}$$

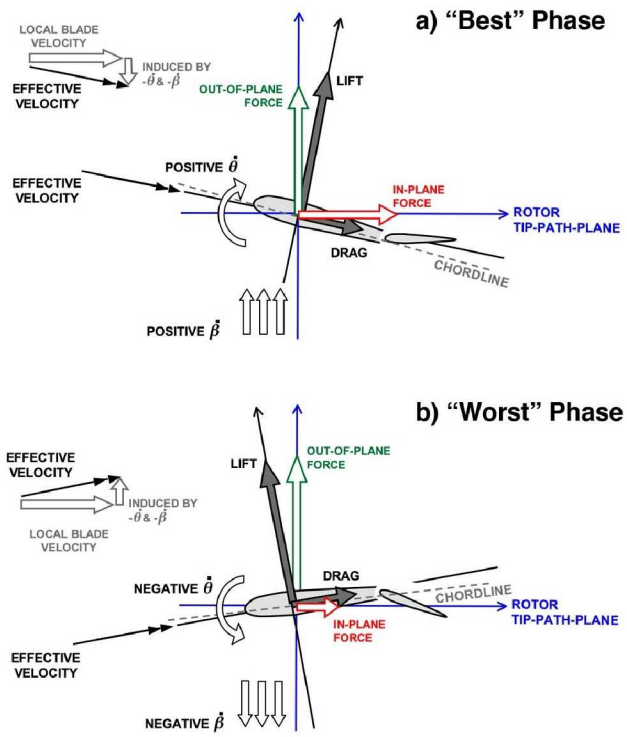

Figure 12. Effects of active flap on blade aerodynamic forces: a) reduced noise-mode, b) increased noise-mode.

Single harmonic flap input: Amplitude sweep

Amplitude sweeps of active flap deflections were also conducted during the wind tunnel test to explore further in-plane noise reduction possibilities. Figure 13 shows the results for 2P, 3P and 4P flap actuation where the active flap phase, at each frequency, was fixed at its "best" phase setting. Acoustic data for flap amplitudes ranging from 0.7° to 2.0° were collected, depending on rotor balance and blade load safety tolerances. Within this range of flap amplitudes, Figure 13 shows that increasing flap amplitudes at 3P and 4P achieved more noise reductions. Best noise reduction of 5.1 dB and 5.7 dB was achieved at 2.0° flap amplitude at 3P, and at 1.3° flap amplitude for 4P, respectively. Beyond these measured flap amplitudes, extrapolated trends suggest that there is an optimum point whereby further increase in flap amplitude does not necessarily result in more noise reductions. This is shown to be the case for 2P where noise reduction margin diminishes from 2.8 dB at 1.5° flap amplitude to 2.0 dB at 2.0° flap amplitude.

Predicted levels in Figure 13 illustrate good correlations with measured data at small flap amplitudes up to 1.0°. At larger flap amplitudes, discrepancies between predicted and measured noise reduction levels are quite significant. An example is the 2P flap motion case that demonstrated up to 4.5 dB differences at about 2.0° flap amplitude (Figure 13a). Similarly, predicted noise levels deviate from measurement by about 3 dB for the 4P case at the largest 1.3° flap amplitude setting.

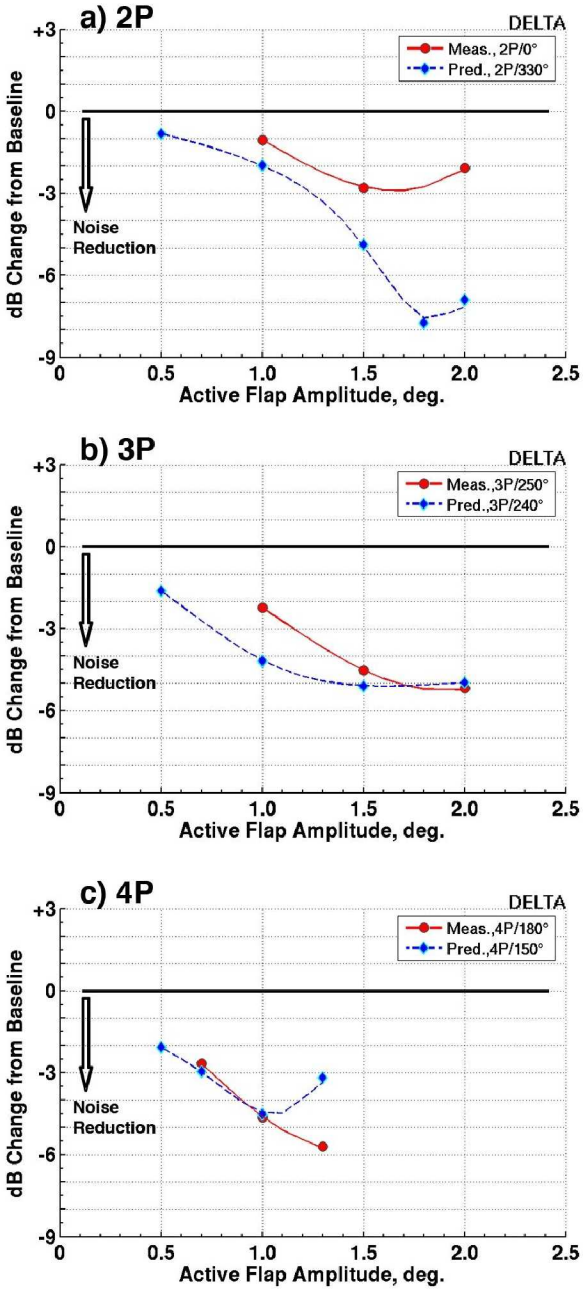

Figure 13. Changes in LFSPL (from baseline) at microphone M13 as a function of active flap amplitude: a) 2P, b) 3P, c) 4P.

Figure 14 illustrates the "best" phase, "best" amplitude measured acoustic time histories (microphone M13) for all the single harmonic flap actuation cases studied in this paper. Deploying active flaps in these manners were found to reduce negative acoustic pressure peaks by at least 50%. These reductions, however, did not occur uniformly for the pulses emanating from all five blades. Compared to the baseline acoustic signature, and also to the more benign 2P case, actuating the trailing-edge flap at 3P and 4P appear to generate much stronger blade-to-blade differences. In addition, these higher active flap frequencies also seem to incur higher MFSPL levels that denote added acoustic energy in the higher blade-passing harmonics.

For all these "best" phase, "best" amplitude cases, the flap deflection and blade dynamics trends are consistent with those reported in the previous section (Figure 15). With exception of chord-wise bending, it appears that steeper gradients in flap deflection, torsion and flap-wise bending (near 90° blade azimuth) result in higher levels of noise reduction. Although the reason is unknown, it is likely that these steeper gradients induce stronger temporal variations that facilitates in generating "anti-noise" pulses of larger amplitude that cancel more of the negative pressure peak.

IMPLICATIONS

The "anti-noise" profiles, generated by active flap motions, at microphone M13 are illustrated in Figure 16. These profiles are calculated by subtracting the measured baseline time history from the "best" phase, "best" amplitude conditions shown in Figure 14. Compared to baseline signature, single-harmonic active flap actuation, at these amplitude/frequency/phase combinations, yielded carefully timed positive acoustic pressure peaks that resulted in suppression of the dominant negative pressure peaks associated with in-plane thickness noise. The synthesized "anti-noise" profiles are of similar pulse-widths compared to baseline signature – with the 2P flap providing the broadest "anti-noise" best matched the baseline negative pressure peak. Gradual narrowing of the pulse-widths at 3P and 4P flap settings suggest that operating active flaps at higher frequencies may not be apt in canceling the relatively width negative pressure peak by any significant margins.

However, as shown in Figure 16, higher 3P and 4P flap frequencies yielded larger "anti-noise" amplitudes that cannot be replicated by 2P flap actuation with any realistic active flap deflection amplitudes. These conflicting demands suggest the likelihood of a delicate compromise in the active flap actuation schedule (i.e. between "anti-noise" pulse-width and amplitude requirements) that would best suppress the baseline negative pressure peak.

Operating active flap at a single harmonic frequency also has limited use in achieving sound cancellation away from the negative pressure peaks. Spurious fluctuations are created off to the sides of the "anti-noise" positive pressure peak that added to baseline noise. This is largely in part due to active flap motions that were confined to harmonic cyclical deflections and not the time-varying deflections required to generate the exact and opposite "anti-noise" pulse.

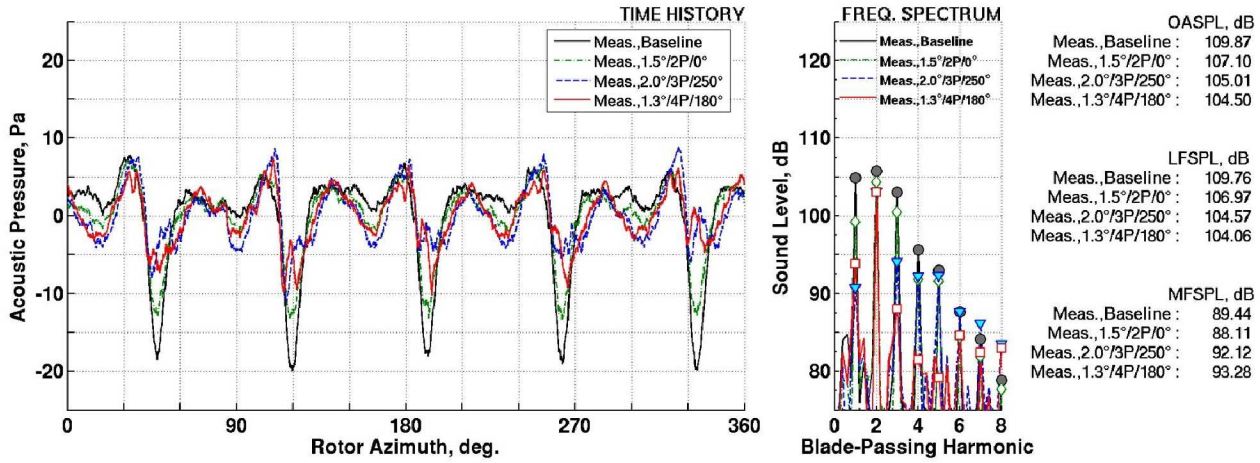

Figure 14. Measured acoustic time histories and frequency spectra at "best" phase, "best" amplitude conditions (microphone M13): a) 1.5°/2P/0°, b) 2.0°/3P/250°, c) 1.3°/4P/180°.

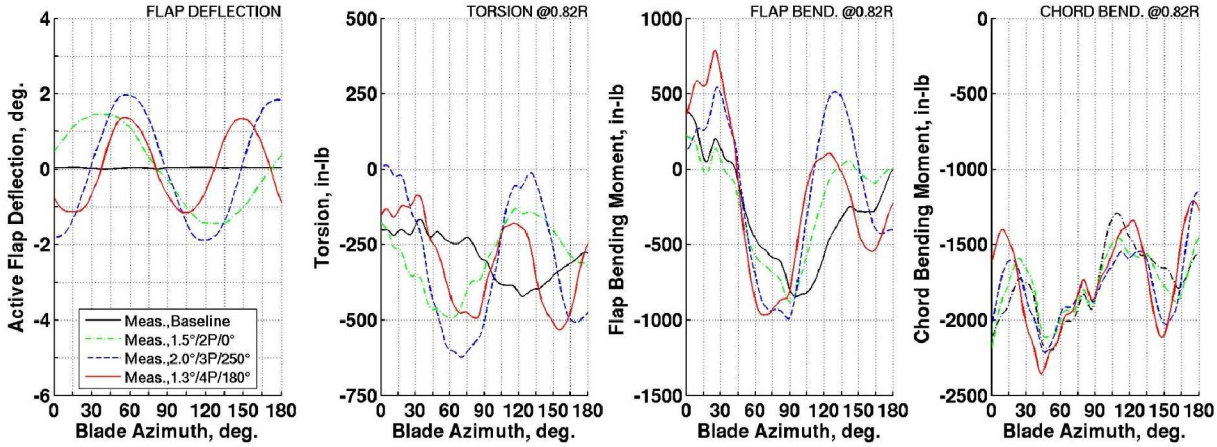

Figure 15. Measured (blade 1) flap deflection and blade dynamics (at 0.82*R*) for "best" phase, "best" amplitude conditions: a) 1.5°/2P/0°, b) 2.0°/3P/250°, c) 1.3°/4P/180°.

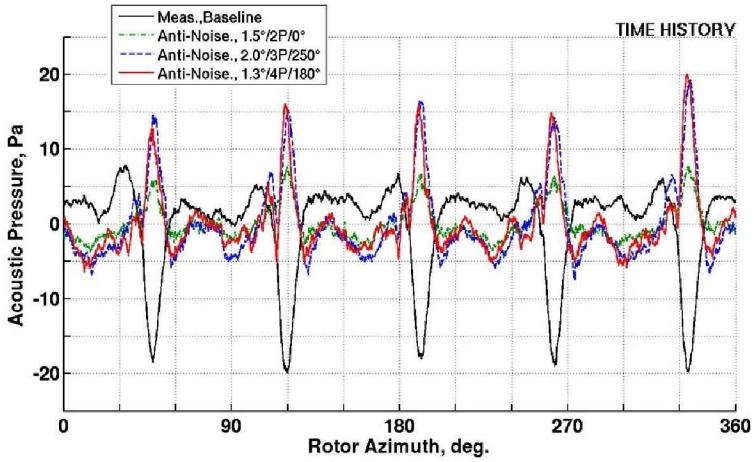

Figure 16. "Anti-noise" profiles (microphone M13) generated by "best" phase, "best" amplitude active flap conditions: a) 1.5°/2P/0°, b) 2.0°/3P/250°, c) 1.3°/4P/180°.

Reduction in aural detection distance associated with these "best" phase, "best" amplitude cases are shown in Figure 17. These calculations were obtained from the "I Can Hear It Now" (ICHIN) code (ref. ?) with source noise inputs derived from the measured acoustic time histories shown in Figure 14. Prior to implementation, the measured time histories were extrapolated to 500-feet and Doppler-shifted to simulate main rotor-only, flyover noise condition. Processed narrow-band spectral levels were subsequently fed into ICHIN to assess aural detection probability as a function of vehicle-to-observer distance and frequency. For all these cases, aural detection assessments were conducted with respect to standard low reference ambient noise at standard atmospheric conditions.

Figure 17a illustrates the ICHIN output for baseline condition. Horizontal bars indicating the probability of detection, and their accompanying distances (x-axis), are illustrated as a function of the source frequency band (y-axis). Longer bars depict less desirable circumstances where the vehicle can be detected further away. For simplicity, the overall aural detection metric is based on the largest distance associated with 50% detection probability – which is 0.558 for the baseline case shown here.

For the active flap cases illustrated in Figure 17b through 17d, reduced in-plane, low frequency source noise is shown to directly reduce detection distance. The best cases, at 3P and 4P (with approximately 5 to 6 dB low frequency noise reduction), enabled detection distance to be reduced by about 18%, while the 2P case (with 2.8 dB noise reduction) only provided 7%. It is also of interest to note that reduction in detection distance at lower frequencies for 3P and 4P, are accompanied by increases at higher frequencies. This is due to stronger mid-to-higher frequencies source noise (MFSPL) generated as discussed before. Although not enough to set the overall detection distance here, it is likely to become an issue at higher frequency flap settings.

The impact of reduced noise operations on rotor performance and hub vibrations are illustrated in Figure 18. For the three "best" phase, "best" amplitude conditions identified in this paper, reduction in in-plane noise and in aural detection distance is accompanied by reduction in rotor (lift-to-drag ratio) performance of up to 3%. This is attributed to increase in shaft torque associated with increase in the chord-wise force required for noise cancellation. The same mechanism introduces a one-per-rev variation in blade shear loads that resulted in a significant increase in in-plane (drag and side) hub vibration levels. While the performance loss is relatively benign, the huge increase in hub shear forces is a cause for concern for rotor fatigue and cabin comfort, and must be addressed prior to using active flaps for reduced in-plane noise operations on helicopter platforms.

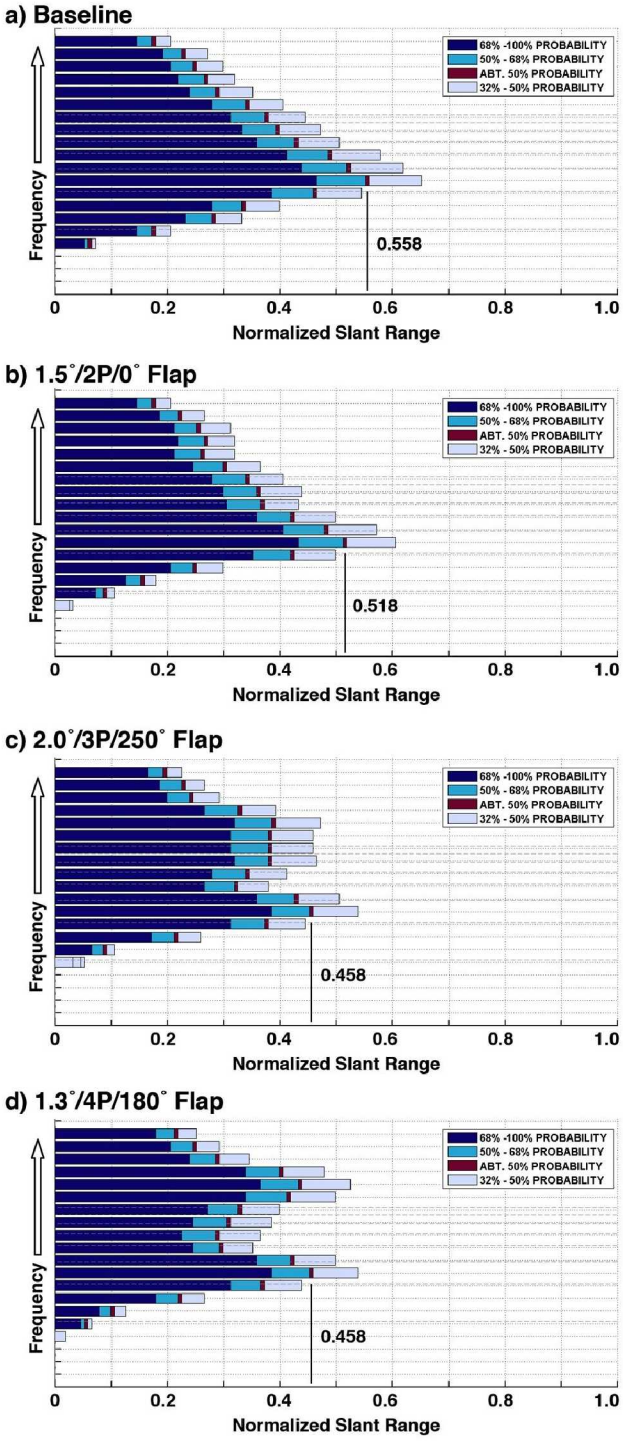

Figure 17. ICHIN results: a) Baseline, b) 1.5°/2P/0°, c) 2.0°/3P/250°, d) 1.3°/4P/180°.

OTHER LIMITATIONS & ISSUES

Aside from performance losses and high vibration levels, there are other limitations that question the ability of this noise reduction strategy to be applied in an advantageous and controlled manner.

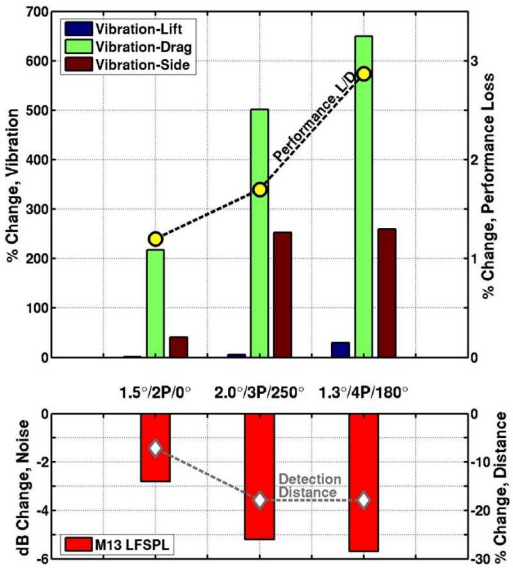

Figure 18. In-plane noise reduction implications on detection distance and rotor performance

Directionality issues. Directivity coverage is a concern, as the concept of reducing free-field noise via introducing an additional "anti-noise" source is known to be problematic. Tuning the active flap to reduce noise at one location is likely to increase noise elsewhere – generating spatial pockets of high and low noise levels where the "anti-noise" can either, add or cancel the original source. Figure 19 illustrates this critical directionality issue via predicted noise level changes for a 1.0°/4P/150° active flap case in a spatial region 10*R* forward of the rotor. Changes in the low frequency sound pressure levels (LFSPL) from baseline are plotted in ±45° azimuth window from the forward station, and for –30° to 15° elevation angle with respect to the horizon. While the noise directly forward, in-plane of the rotor is shown to be reduced, it demonstrated also that higher noise levels can incur elsewhere at other locations. The "hotspot" formed on the advancing side, near 140° azimuth, is an artifact of the single harmonic-driven flap introducing poorly phased "anti-noise" signatures that resulted in undesirable noise amplification at this location. In contrast, the second "hotspot" near 30° below the horizon is generated from local blade lift variations introduced by active flap deployment. As shown in Figure 20 for the out-of-plane microphone (M1) for the 2.0°/3P/250° flap actuation schedule, this increase in noise over baseline can be rather significant. Naturally, these observations imply limited use of single-harmonic, single active flap actuation for global noise reductions.

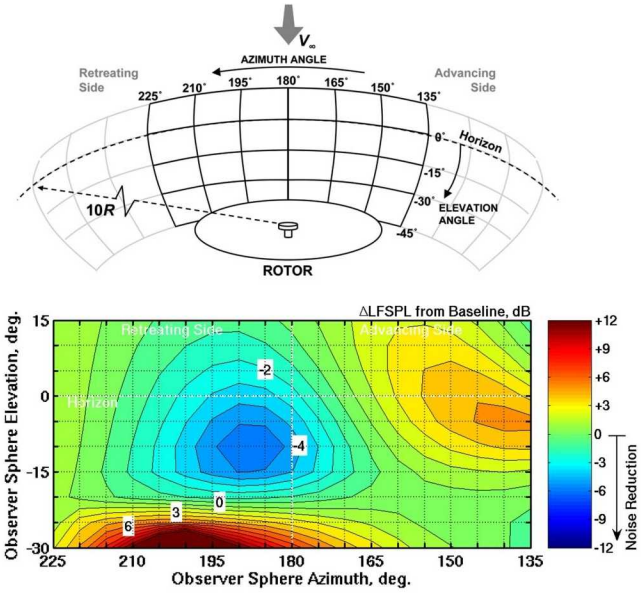

Figure 19. Predicted change in LFSPL from baseline at forward, in-plane locations 10*R* from the rotor.

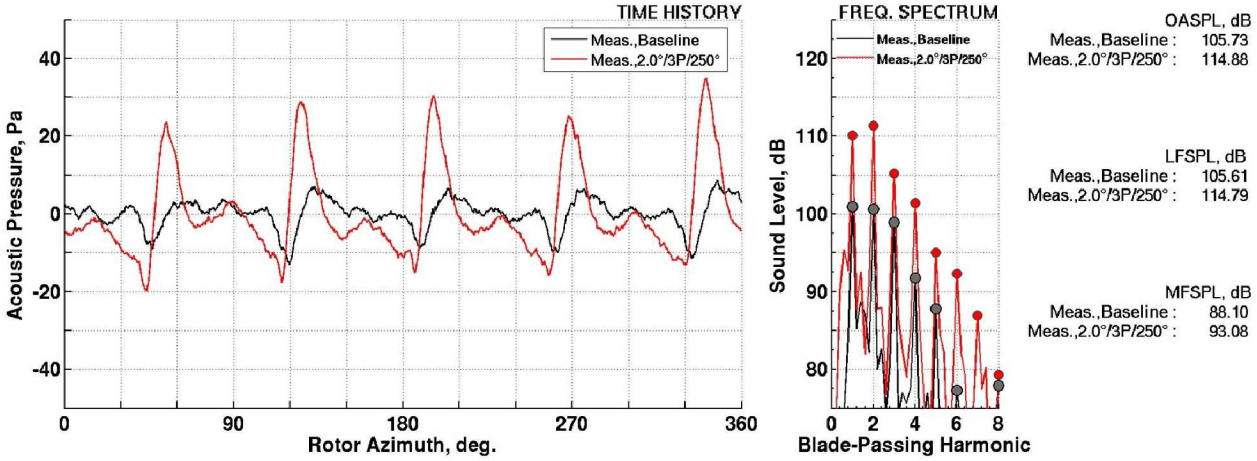

Figure 20. Measured acoustic time histories and frequency spectra at out-of-plane microphone (M1).

Feasibility across extended flight envelope. With measurement obtained at only one advance ratio (0.30) in this test, it is unclear if the Boeing-SMART active flaps are robust enough to deliver sufficient cancellation authority at higher airspeeds. The negative thickness noise peak is increases considerably with airspeed, especially near delocalization Mach numbers[9], and would demand larger amplitudes and/or markedly different actuation strategies to generate the required "anti-noise".

Flap actuation issues. It is necessary to have a well-designed close loop flap controller to achieve repeatable and accurate active flap-induced benefits. This point was demonstrated during the Boeing-SMART test whereby active flaps were actuated using a pre-set voltage inputs in open loop mode and also commanded by a close loop controller to deliver similar flap actuation schedules. Figure 21a shows the instantaneous and averaged flap deflection for all five blades at baseline condition measured during sixty-four revolutions of data acquisition. Under open loop mode, the active flaps, which were not mechanically locked out, were found to oscillate by up to 2° with significant amount of variations between each revolution. As shown in Figure 21a, this is greatly suppressed when the close loop flap controller was implemented. Surprisingly, the effect on noise at microphone M13 is minimal, with only 1.3 dB differences in the measured LFSPL at baseline condition. Although this is somewhat true for the 3P case as well (Figure 21b), results for 4P flap actuation (Figure 21c) shows significant differences in radiated rotor noise using open and close loop flap control. This was attributed to the "soft" blade torsion mode, occurring near four-per-rev frequency, which incurred large blade motion instabilities with 4P flap deflections inputs. Close loop flap controller must be used to maintain tracking in this case to obtain stable and repeatable results.

IDEAL ACOUSTICS CONTROL

Although reduced in-plane, low frequency noise is demonstrated via the Boeing-SMART flap, the proposed noise cancellation concept is not limited to only this type of "on-blade" active control device. Based on present studies, anticipated demands for greater noise reductions, over a sufficiently wide area, calls for better "on-blade" controls and/or actuation strategies.

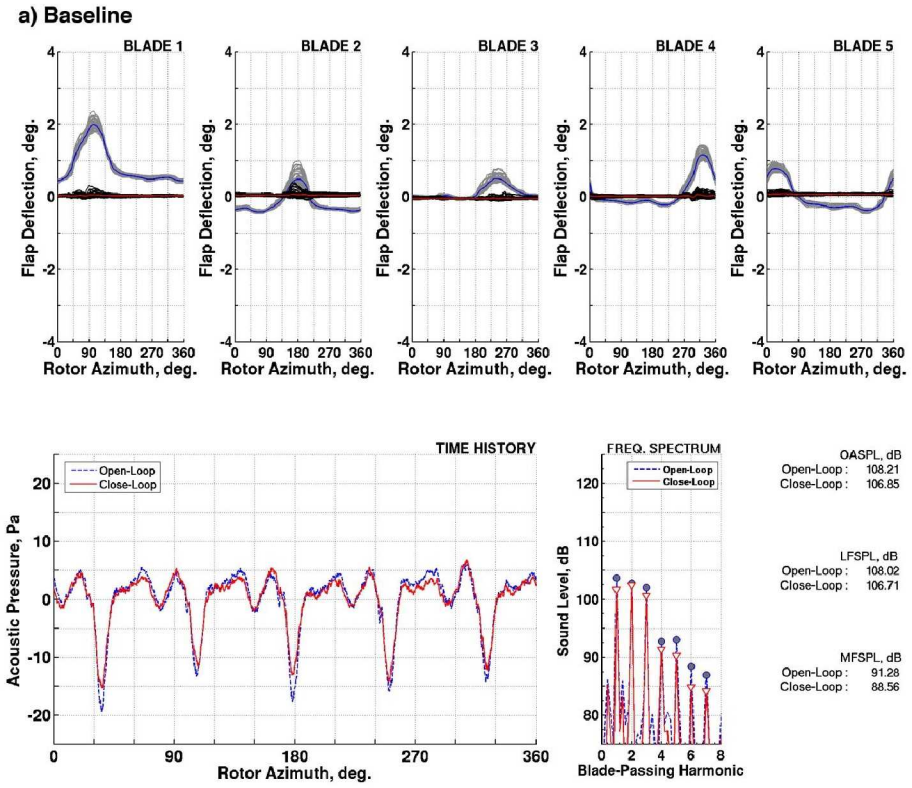

Figure 21. Variation in noise measurement (microphone M13) due to open and close loop flap controller: a) baseline, b) 1.0°/3P/60°, c) 1.0°/4P/180°.

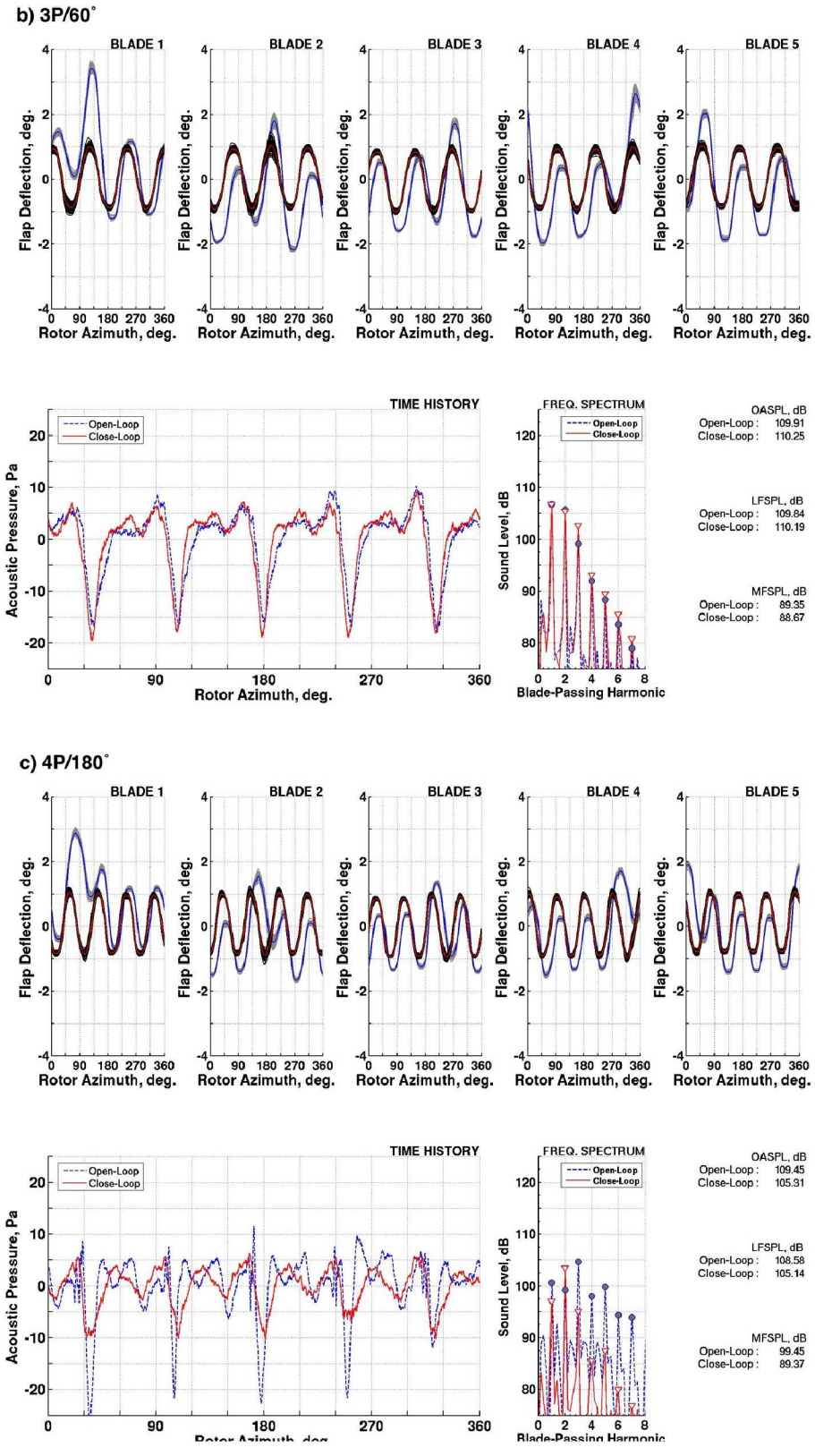

Figure 21. continued

Foremost is the need for a control device that only affects in-plane (chordwise) forces, and not the out-of-plane forces primarily associated with lift, to avoid increase in noise around the rotor. Use of multiple devices, distributed along the blade span, to enable better-phased and better "anti-noise" pulse shapes is highly desirable for larger noise reduction and for improved directionality considerations. In addition, it would also be beneficial to configure these devices to not operate at a single discrete harmonic frequency, but in a time-varying fashion that mimics the shape and form of the thickness noise pulse (with opposite sign). Doing so allows for more complete and uniform cancellations across the low frequency bands and, simultaneously, minimizes noise residuals in higher frequencies.

CONCLUSIONS

Acoustic measurement obtained from the joint DARPA/Boeing/NASA/Army/Air Force test in the National Full-Scale Aerodynamic Complex's 40- by 80-ft anechoic wind tunnel demonstrated that it is possible to reduce in-plane, low frequency noise of the Boeing-SMART rotor via carefully chosen active flap deflection schedules. Results are shown for a condition corresponding the level flight cruise at an advance ratio of 0.30. Depending on the amplitude, frequency and phase of the (single harmonic) active flap actuation schedule, up to 6 dB of noise reduction in the first six blade-passing harmonics at a single far-field microphone are reported. For the cases shown in this paper, best noise reduction is reported when the active flap was commanded at 1.3°/4P/180°.

The underlying mechanism of these reduced in-plane, noise levels is attributed to the ability of active flaps in generating appropriate "anti-noise" pulses that partially cancel the negative pressure peak commonly associated with steady thickness noise. Measurements showed that the "anti-noise" is generated via increasing in-plane forces in the vicinity near the advancing side near 90° blade azimuth. This is achieved by re-orienting the local lift vector associated with active flap-induced changes in blade torsion and blade flapping characteristics. These current observations substantiated hypothesis and pre-requisites[2,7] , previously postulated, for achieving meaningful in-plane noise reduction.

Reduced in-plane, low frequency noise levels are shown to directly reduce aural detection distance through ICHIN analyses. A decrease of 18% in detection distance was found to accompany source noise reductions of about 6 dB. ICHIN results also demonstrated the possibility of higher source noise frequencies establishing the detection distance with active flaps.

High vibration levels are incurred during reduced in-plane noise operations. Vibratory loads primarily results from increase in in-plane shear forces driven by the need to increase in-plane forces on the advancing side of the rotor to achieve noise cancellation. Rotor performance penalties are quite small, with less than 3% increase in shaft torque compared to the baseline case with no active flap deployed.

Conventional comprehensive rotor analysis and acoustic analogy-based codes are capable of providing good correlations with measured noise data at low flap amplitude settings. Predicted noise levels at higher flap deflections (greater than 1.0 degree) deviate from measured values in both amplitudes and trends.

Limitations of this noise reduction strategy, discussed in the paper, center on directivity concerns. Global noise reduction is not possible as the underlying physics of this approach relies on phase cancellation of steady thickness noise using modified loading noise generated by the active flaps. This yielded regions with high and low noise intensities that are indicative of constructive and destruction interference. Use of active flap is not necessarily best for reducing in-plane noise. This is because it makes use of aerodynamic lift forces to achieve desirable in-plane noise cancellation, at the expense of generating more noise at out-of-plane observer locations. It is recommended that a "drag"-only controller be used to achieve better global low frequency noise reduction.

ACKNOWLEDGMENTS

Many thanks to the Boeing-SMART rotor test crew, including the participants from NASA Ames, Army/AFDD, Air Force/NFAC, and M.I.T. for enabling acquisition of the comprehensive acoustics database used in this study. In particular, the authors would like to thank:

- Dr. Fredrich Straub and Mr Roger Smith (Boeing) for their helpful discussions on the SMART rotor,
- Mr. Cahit Kitaplioglu and Mr. Benton Lau (NASA Ames) for data collection and for their participation in acoustics calibration of the 40- by 80-ft test section,
- Dr. Wayne Johnson (NASA Ames) for providing the CAMRAD-II calculations,
- Mr. Jan vanArken and Ms. Lei Yang (NFAC) for their work on real-time acoustic post-processing software,
- Mr. Thomas Maier (AFDD) and Dr. William Warmbrodt (NASA Ames) for their support on this research topic, and
- Prof. Fredric Schmitz (University of Maryland) for his elaborate discussions and insights on rotor acoustics.

REFERENCES

1. Crawford, C. Jr., "Noise Requirements from A Military Point of View," NASA CP-2052, May 1978, pp. 33-44.

2. Sim, B. W., "Suppressing In_Plane, Low Frequency Helicopter Harmonic Noise with Active Controls," Presented at the American Helicopter Society San Francisco Bay Area Chapter's Aeromechanics

Specialist's Meeting, Fisherman's Wharf, CA, January 2008.

3. Yu, Y. et. al., "The HART-II Test: Rotor Wakes and Aeroacoustics with Higher-Harmonic Pitch Control (HHC) Inputs – The Joint German/French/Dutch/US Project," Presented at the American Helicopter Society 58th Annual Forum, Montreal, Canada, June 11-13, 2002.

4. Jacklin, S. A. et. al., "Reduction of Helicopter BVI Noise, Vibration and Power Consumption Through Individual Blade Control," Presented at the American Helicopter Society 51st Annual Forum, May 1995.

5. Marcolini, M, A et. al., "Control of BVI Noise Using an Active Trailing-Edge Flap," Presented at the 1999 American Helicopter Society San Francisco Bay Area Chapter's Vertical Lift Aircraft Design Conference, San Francisco, CA.

6. Booth, E. R. Jr. and Wilbur, M. L., "Acoustic Aspects of Active-Twist Rotor Control," Presented at the American Helicopter Society 58th Annual Forum, Montreal, Canada, June 11-13, 2002.

7. Schmitz, F. H. and Gopalan, G., "High-Speed Impulsive Helicopter Noise Reduction Possibilities Through On-Blade Acoustic Control," Presented at the International Forum on Rotorcraft Multidisciplinary Technology Organized by AHS International and the Korean Society for Aeronautical and Space Sciences, Seoul, Korea, October 15-17, 2007.

8. Straub, F. K. ------ SMART Overview

9. Schmitz, F.H., "Rotor Noise," Chapter 2 in book authored by Hubbard, H. H., *Aeroacoustics of Flight Vehicles, Theory and Practice, Vol. 1: Noise Sources*, Published for the Acoustical Society of America through the American Institute of Physics, 1995.

10. Deming, A. F., "Noise from Propellers with Symmetrical Sections at Zero Blade Angle, II., NACA TN-679, December 1938.

11. Gutin L., "On the Sound Field of a Rotating Propeller," NACA TM-1195, October 1948.

12. Farassat, F. and Succi, G. P., "The Prediction of Helicopter Rotor Discrete Frequency Noise," *Vertica*, Vol. 7, No. 4, pp. 309-320, 1983.

13. Jacklin, S. A., Lau, B. H., Nguyen, K. Q., Smith, R. L. and McNulty, "Full-Scale Wind Tunnel Test of the McDonnell Douglas Five-Bladed Advanced Bearingless Rotor: Performance, Stability, Loads, Control Power, Vibration and HHC Data," Presented at the American Helicopter Society Aeromechanics Specialists Conference, San Francisco, California, January 19-21, 1994.

14. Schmitz, F. H., Allmen, J. R., and Soderman, P. T., "Modification of the Ames 40- by 80-Foot Wind Tunnel for Component Acoustic Testing for the Second Generation Supersonic Transport," NASA TM-108850, October 1994.

15. Soderman, P. T., Jaeger, S. M., Hayes, J. A. and Allen, C. S., "Acoustic Quality of the 40- by 80-Foot Wind Tunnel Test Section After Installation of a Deep Acoustic Lining," NASA TP-2002-211851, November 2002.

16. Allen, C. S., Jaeger, S. M. and Soderman, P. T., "background Noise Sources and Levels in the NASA Ames 40- by 80-Foot Wind Tunnel at the Turn of the Century: A Status Report," NASA TP-2003-212259, November 2003.

17. Johnson, W. R., "Rotorcraft Aerodynamics Models for a Comprehensive Analysis," Presented at the American Helicopter Society Forum, Washington, D.C., May 1998.

18. Kottapalli, S. and Straub, F. K., "Correlation of SMART Active Flap Rotor Loads," Presented at the American Helicopter Society 65th Forum, Grapevine, Texas, May 27-29, 2009.

19. Shirey, J. S., Brentner, K. S., Chen, H.-N., "A Validation Study of the PSU-WOPWOP Rotor Noise Prediction System," Presented at the 45th AIAA Aerospace Sciences Meeting and Exhibit, Reno, Nevada, January 8-11, 2007.

20. ICHIN